DOKUZ EYLÜL UNIVERSITY
GRADUATE SCHOOL OF NATURAL AND APPLIED SCIENCES

MINERALOGICAL AND GEOCHEMICAL STUDY OF KIZILTEPE Au-Ag DEPOSIT AND SURROUNDING PROSPECTS IN THE SINDIRGI-DURSUNBEY DISTRICT, BALIKESİR, WESTERN TURKEY

by

Seda TEZEL TUFAN

September, 2005
İZMİR

MINERALOGICAL AND GEOCHEMICAL STUDY OF KIZILTEPE Au-Ag DEPOSIT AND SURROUNDING PROSPECTS IN THE SINDIRGI-DURSUNBEY DISTRICT, BALIKESİR, WESTERN TURKEY

A Thesis Submitted to the
Graduate School of Natural and Applied Sciences of Dokuz Eylül University
In Partial Fulfillment of the Requirements for the Degree of Master of Science
in Geological Engineering, Economic Geology Program

by

Seda TEZEL TUFAN

September, 2005
İZMİR

M.Sc THESIS EXAMINATION RESULT FORM

We have read the thesis entitled **"MINERALOGICAL AND GEOCHEMICAL STUDY OF KIZILTEPE Au-Ag DEPOSIT AND SURROUNDING PROSPECTS IN THE SINDIRGI-DURSUNBEY DISTRICT, BALIKESİR, WESTERN TURKEY"** completed by **SEDA TEZEL TUFAN** under supervision of **PROF. DR. ISMET OZGENC** and we certify that in our opinion it is fully adequate, in screpe and in quality, as a thesis for the degree of Master of Science.

Prof. Dr. İsmet ÖZGENÇ

_____

Supervisor

Prof Dr Uğur KÖKTÜRK

_____

(Jury Member)

Yrd. Dç. Tolga OYMAN

_____

(Jury Member)

_____

Prof.Dr. Cahit HELVACI
Director
Graduate School of Natural and Applied Sciences

ACKNOWLEDGEMENTS

I thank my supervisior, Prof.Dr Huseyin Yilmaz, for giving me the opportunity to work in a very interesting area, and for his support and guidance throughout my M.Sc. study at Sindirgi - Balikesir.

Prof.Dr. Ismet Ozgenc is thanked in particular for his interest and support of the project during my study.

I am greatful to Assistant Prof. Erhan Akay and Assistant Prof. Fatma Nuran Sönmez for helping me on different parts of the study.

I would like to thank my administrator in Greater City of İzmir Municipality Sedat BAYLAN and my chef İbrahim KARATAS for their support this study.

Thanks to the Galata Madencilik San ve Tic.Ltd.Şti. for providing me with the financial means to complete this project.

And finally, thanks to my husband M.Sc. Geologist Volkan Tufan and parents who endured this long process with me, always offering support and love.

Seda TEZEL TUFAN

MINERALOGICAL AND GEOCHEMICAL STUDY OF KIZILTEPE Au-Ag DEPOSIT AND SURROUNDING PROSPECTS IN THE SINDIRGI-DURSUNBEY DISTRICT, BALIKESİR, WESTERN TURKEY

ABSTRACT

This project aims to undertake an integrated mineralogical, geochronological, alteration, geochemical and fluid inclusion study of the Kiziltepe Au-Ag deposit that located at approximately 63 km southeast of Balıkesir in western Turkey and surrounding prospects. The aim of this investigation is to constrain the origin and evolution of the deposit to address the following fundamental questions such as the source(s) of fluids and the temporal and spatial relationship between volcanism and adularia-illite (sericite) alteration, and Au mineralization. The study area displays typical low temperature epithermal textures, including crustiform banding and hydrothermal breccias. Argillic alteration is characterized by smectite and kaolinite, commonly replacing plagiocalse, yielding an altered rock depleted in Ca and Na, among others. Accordingly fluid inclusion results, Kızıltepe have average fluid inclusion homogenization temperatures around 206°C, Kavaklıdüz and Karadüz both contain significantly higher average homogenization temperatures 252°C, Kepez have 216°C. As for % NaCl results, four areas at issue (Kiziltepe, Kepez, Karadüz and Kavaklidüz) have salinity rate between %1 and %2. All of the results show the epithermal system. Geochemical variations in altered wall rocks are generally charracterized by two-fold enrichments in K, Rb, Cs, Cr. The wall rock enrichments in Au, Ag, As. Positive correlation coefficients of Au with Ag and Sb in epithermal quartz veins are strong, all of which greater than 0,50. Correlations between Au-As and Au-Cu are very weak whereas no correlation occurs between Ag and Cd. There are very strong correlation coefficients of Ag with Au (R=0,93) and Sb (R=0,79). All of age $^{40}Ar/^{39}Ar$ results suggested that the age of lower ignimbrite is 19.82 ± 0.14 Ma, upper ignimbrite is 18.96 ± 0.11 Ma and mineralization is 8.27 ± 0.11 Ma.

Keywords: Sindirgi, alteration, geochemistry, age, gold mineralization.

SINDIRGI-DURSUNBEY YÖRESİNDEKİ (BALIKESİR-BATI ANADOLU) KIZILTEPE Au-Ag YATAĞI VE ÇEVRESİNDEKİ PROSPEKTLERİN MİNERALOJİK-JEOKİMYASAL ÇALIŞMASI

ÖZ

Bu proje, Türkiye'nin batısında, Balıkesir'in yaklaşık 63 km güneydoğusunda bulunan Kiziltepe Au-Ag yatağının mineralojik, jeokronolojik, alterasyon, jeokimyasal ve sıvı kapanım çalışmalarının bütününü ele almaktadır. Bu araştırmanın amacı, yatağın köken ve oluşumuna ait, akışkanların kaynağı, volkanizma ile adularya-illit (serisit) alterasyonu ve altın mineralizasyonu arasındaki mekansal ve temporal bağı tanımlamak gibi birincil sorulara yanıt göstermektir. Çalışma alanı, kolloform/kabuksu şekilli bantlaşmai hidrotermal breş gibi düşük derece epitermal dokuları gösterir. Alterasyon mineralleri baskın olarak simektit, kaolinittir. Sıvı kapanım sonuçlarına göre Kızıltepe'nin homojenleşme sıcaklığının ortalaması yaklaşık 206°C, Kavaklidüz ve Karadüz'in yaklaşık 252°C ve Kepez'in ki 216°C olarak saptanmıştır. Söz konusu dört alanın (Kızıltepe, Kepez, Karadüz ve Kavaklıdüz) tuzluluğu %1 ve %2 arasındadır. Tüm sonuçlar epithermal tip yatağı işaret etmektedir. Altere yan kayaçda jeokimyasal değişimler K, Rb, Cs ve Cr de iki kat zenginlelme ile karakterize edilir. Yan kayaç Au, Ag ve As de zenginleşme gösterir. Au ile Ag (R=0,93) ve Sb (R=0,79) arasında yuksek pozitif korelasyon mevcuttur. Korelasyon katsayısı 0,5 in üzerindedir. Au-As ve Au-Cu arası korelasyon katsayısı çok düşüktür, Ag ile Cd arasında korelasyon bulunmamaktadır. ^{40} Ar/^{39} Ar sonuçlarına göre alt ignimbiritin yaşı 19.82 ± 0.14 Ma, üst ignimbiritin yaşı 18.96 ± 0.11 Ma ve mineralizasyonun yaşı 8.27 ± 0.11 Ma olarak saptanmıştır.

Anahtar sözcük: Sındırgı, alterasyon, jeokimya, yaş, altın mineralleşmesi.

CONTENTS

Page

CHAPTER ONE
INTRODUCTION

1.1. Location and Access

Sındırgı is located at approximately 63 km southeast of Balıkesir in western Turkey. The Study area is surrounded by Dursunbey, Bigadic on the north, Demirci, Gördes, Akhisar (Manisa) on the south, Kırkağaç (Manisa) on west and Simav (Kütahya) on the east (Figure 1.1).

Figure 1.1 Balıkesir-Sindirgi location map.

1.2. Purpose and Methods

This project aims to undertake an integrated mineralogical, geochronological, alteration, geochemical, fluid inclusion of the Kiziltepe Au-Ag deposit and surrounding prospects. These prospects, occurring at different elevations, are the best-exposed low-sulfidation deposits in the Sindirgi region. The aim of this investigation is to constrain the origin and evolution of the deposit to address the following fundamental questions

such as the (a) source(s) of fluids and (b) the temporal and spatial relationship between volcanism and adularia-illite (sericite) alteration, and Au mineralization. The enhancement of exploration criteria for similar epithermal deposits in the Sindirgi-Dursunbey region is also another aim of this study.

Fieldwork was carried out between September and October 2006. Samples were taken from quartz vein at Kiziltepe, Kepez, Karadüz and Kavaklidüz prospects. The laboratory and office work involved petrographic investigation (fluid inclusion) of 14 optical polished and 65 thin sections on ore samples from outcrop and diamond drill cores. Geochemical analyses were done from 10 samples by ACME Analytical laboratories, Vancouver, Canada. XRD analyses were done at Geothermal Energy Groundwater and Mineral Resources Research and Implementation Center, Isparta, Turkey from 10 samples. 4 Ar/Ar age dating samples were sent to Nevada Isotope Geochronology Laboratory, Las Vegas, USA.

1.3. Previous Studies

The regional geology of Western Turkey, including stratigraphy, structure, geochemistry, geophysics, geochronology, were described. Yılmaz (2002) and Yılmaz et al. (2007) suggested that mineralogy, alteration, and fluid inclusion characteristic of the Ovacık Au-Ag deposit were similar to those of other adularia-sericite type or low-sulfidation epithermal gold deposits elsewhere in the world.

Basement rocks of Western Turkey consist of Paleozoic metamorphic rocks and Mesozoic mélange, comprising clastic and carbonate rocks. These basement rocks are cut by granitic and granodioritic intrusives, and are overlain mainly by calc-alkaline and minor alkaline volcanic rocks, ranging in age from 35 to 23 Ma (Yilmaz, 1989; Ercan et al., 1995). The andesitic volcanic suite is represented by andesite, latite, dacite, rhyodacite lava dome facies, and related volcaniclastic sequences. North–south compression and crustal thickening, caused by the north-

dipping subduction of the neo-Tethys oceanic crust beneath the Pontic arc, occurred between the Eocene and Early Miocene. This was followed by partial melting of the lower crust to produce anatectic granitic melts (Yilmaz, 1989) and subsequent downbending of the north-subducting slab. This process led to the ultimate detachment and loss of the northward-dipping slab, giving way to the establishment of an extensional tectonic regime with widespread Basin and Range-style deformation (orogenic collapse) in western Turkey (Wright, 1996). The Ovacik and Narlica gold-silver deposits occur in this geological framework within the Western Turkey magmatic arc complex, which forms a part of the northward-dipping Tethys subduction system. The magmatic rocks, which are of Eocene to Pliocene age, exhibit calc-alkaline to alkaline compositions and are tectonically linked to episodes of subduction and extension related to the northward movement of the African–Arabian plate (Yılmaz et al., 2007).

CHAPTER TWO

GEOLOGY

2.1 Geological Setting

2.1.1 Regional Geology

Widespread magmatism occurred in western Turkey from late Oligocene to early Miosene time. Several authors have published studies on the magmatic rocks of western Turkey (Ercan et al., 1984; Yılmaz, 1989; McKenzie and Yılmaz, 1991; Seyitoğlu and Scott, 1991, Seyitoğlu et al., 1997; Altunkaynak and Yılmaz, 1998).

The oldest units in the region are metamorphic rocks of Paleozoic age. Magmatic activity in the area began with the emplacement of the Kozak pluton.

Coeval, sheeted, hybapyssal intrusive rocks formed around the pluton. These intrusive rocks are, in turn, surrounded by extrusive rocks, which are partly contemporaneous with the emplacement of granitic rocks during the early Miocene. During the Neogene the region was affected by several extensional events (Zanchi et al., 1990, 1993). The earliest extensional phase (northwest-southwest), which prevailed from middle to late Miocene, gave rise to north-noertheast-south-southwest-trendling to northeast-southwest-trendling grabens. This earliest phase was followed by north-south extension during the early Pliosen to Quaternary. Altunkaynak and Yılmaz (1998) suggested that lavas and sheeted high-level intrusions followed the northeast-southwest and north-south-trending oblique faults to reach the surface.

In western Turkey approximately half of the known epithermal deposits are located in andesitic to dacitic rocks, ranging in age from upper Oligocene to Lower Miocene. Such rocks are associated with a major volcanic episode in western Turkey

related to a brief phase of crustal compression. A smaller number of epithermal deposits are hosted by Palaeozoic mica schists or by Upper Cretaceous marine sedimentary rocks associated with ophiolites of the Izmir-Ankara suture zone. Most epithermal Mineralization is vein or stockwork hosted, while a few deposits contain mineralised breccias and disseminations. The likely age of this epithermal gold Mineralization is Middle to Upper Miocene, corresponding to the period of N-S extensional activity in the region (Company reports, Galata Mad.).

2.1.2 Local Geology

The Sindirgi-Dursunbey province including Au occurrences is underlain by a Paleozoic metamorphic to Mesozoic melange rocks, which are cut by Late Oligocene to Miocene plutonic to hypabyssal granodioritic/granitic intrusives, and dacitic/rhyolitic volcanic rocks. Collectively the members of the Sindirgi magmatic association represent subvolcanic intrusives and the overlying hypabyssal and volcanic rocks appear to have formed in one or more caldera collapse environments (Company reports, 2006) (Figure 2.1).

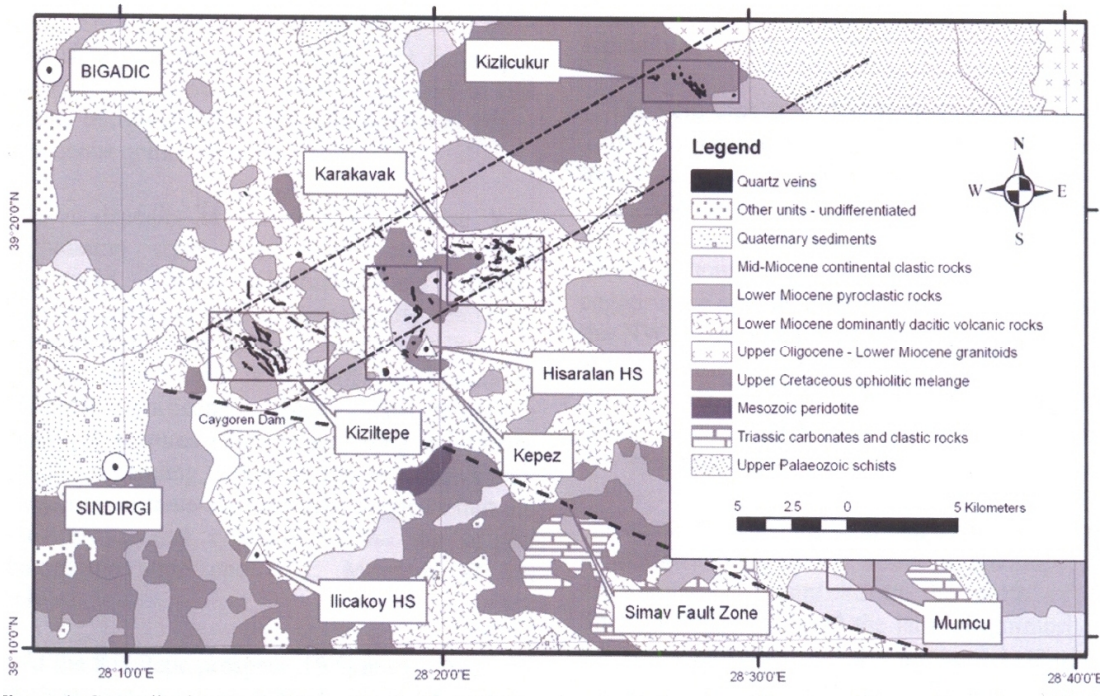

Figure 2.1 Geological map of Sindirgi area (Company reports).

Due to variances in the level of erosion, the metamorphic basement and intrusive rocks predominate in the east whereas the volcanic rocks are extensive in the west. The level of erosion is also reflected by the differences in style of precious and other metal deposits.

The geology of the area is dominated by two major architectural components; The Sindirgi Volcanic Complex (SVC) and The Simav Fault (SF). Dacitic volcanic and overlying dacitic volcanoclastic units of the SVC host the majority of veins at the Kiziltepe and Karakavak prospects. Quartz veins cut rhyodacitic-dacitic ignimbrite underlying most of the prospects.

Four main rock units are distinguished. These are (1) The Pre-Tertiary basement (2) Lower ignimbrite unit (3) Upper ignimbrite unit and (4) Subvolcanic rhyolites (Akay, 2007) (Figure 2.3). The Pre-Tertiary basement, along the road between Çaturtepe and Kepez villages, rock units of the izmir-Ankara Suture Zone constitute the Pre-Tertiary basement unit consisting of the mafic volcanics, serpentinized ultramafic rocks, sandstone and mudstones with rare limestone blocks. The various lithologies in basement association in the area appear lateraly discontinuous boudins and sheared discs in sandy or muddy matrix. Lower ignimbrite unit, red to gray crystal-rich pyroclastic deposits covering a large area from Yusufçami village to Hisaralan hotsprings, along the road between Sindirgi and Simav are classified, in this study, as the Lower ignimbrite unit. This unit is characterized by (1) The Crystal-rich ignimbrite subunit in the lower parts and (2) Ignimbrite breccias in the upper parts. Upper ignimbrite unit, the lower ignimbrite unit is overlain, along an irregular contact, by the Upper ignimbrite unit consisting of white to yellow pumice-rich pyroclastic flow deposits and cropping dominantly out around the northern part of the Kiziltepe Prospect. The Upper ignimbrite unit is characterized by a coarse grained polymictic basal part which is composed of lapilli to boulder-sized fragments derived from the Lower ignimbrite unit and Pre-Tertiary basement rocks set in pumice and crystal fragment-rich ash matrix. Subvolcanic rhyolites; The whole pyroclastic sequence in and around K'z'ltepe Prospect is cut by the white to yellow

rhyolitic stocks cropping out to the south of Yolcupınar village (Figure 2.2). These massive, coherent rhyolites show significant steeply dipping flow foliation along their contact and are surrounded their own autobrecciated periphery zone (Akay, 2007).

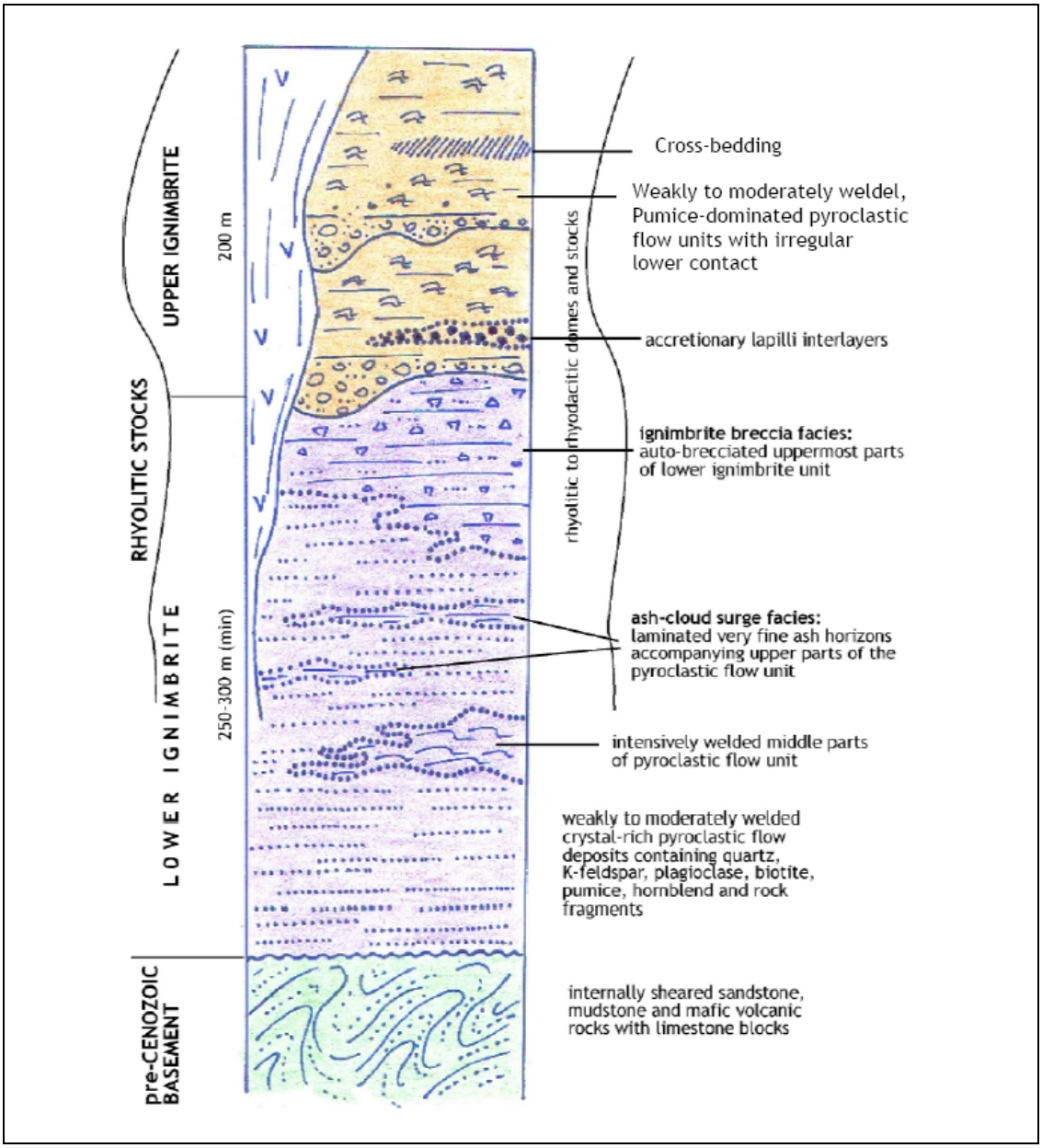

Figure 2.2 Generalized stratigraphic columnar section of the study area (Akay, E., 2007).

2.2 Vein Mineralogy

The Sindirgi area consists mainly of ignimbrites which are subdivided into a) Lower ignimbrite, b) Ignimbrite breccia and Upper ignimbrite. Quartz, plagioclase, biotite and pyrite were observed in most of these lithologies. Iron oxide staining occur within the altered host rock.

The quartz veins occurring mainly in the Lower ignimbrite consist mainly of coarse crystalline quartz and adularia with minor carbonates and chalcedony. Some episodes of quartz deposition and formation of quartz after earlier precipitated calcite are recognized in the veins (Figure 2.3 A). Carbonates, which occur as infilling vugs in the quartz veins are mainly calcite. Lattice bladed quartz texture (Figure 2.3 B) may have formed from pseudomorphous replacement of bladed calcite. These textures are common throughout the Kiziltepe vein system. In general, open-space filling, crustificatiform/colloform banding and multiple quartz brecciate were observed.

2.2.1 Gangue Mineralogy

The quartz veins in the area consist mainly of crystalline quartz, adularia with carbonates and chalcedony. Most deposits in the region comprise low-sulfidation style veins, vein breccias (Figure 2.3 C) and stockworks. Some mineralized and strongly silicified zones are lithostratigraphically controlled and tend to occupy the most brittle unit. Several veins display a variety of textures including colloform-crustiform banding and carbonate replacement.

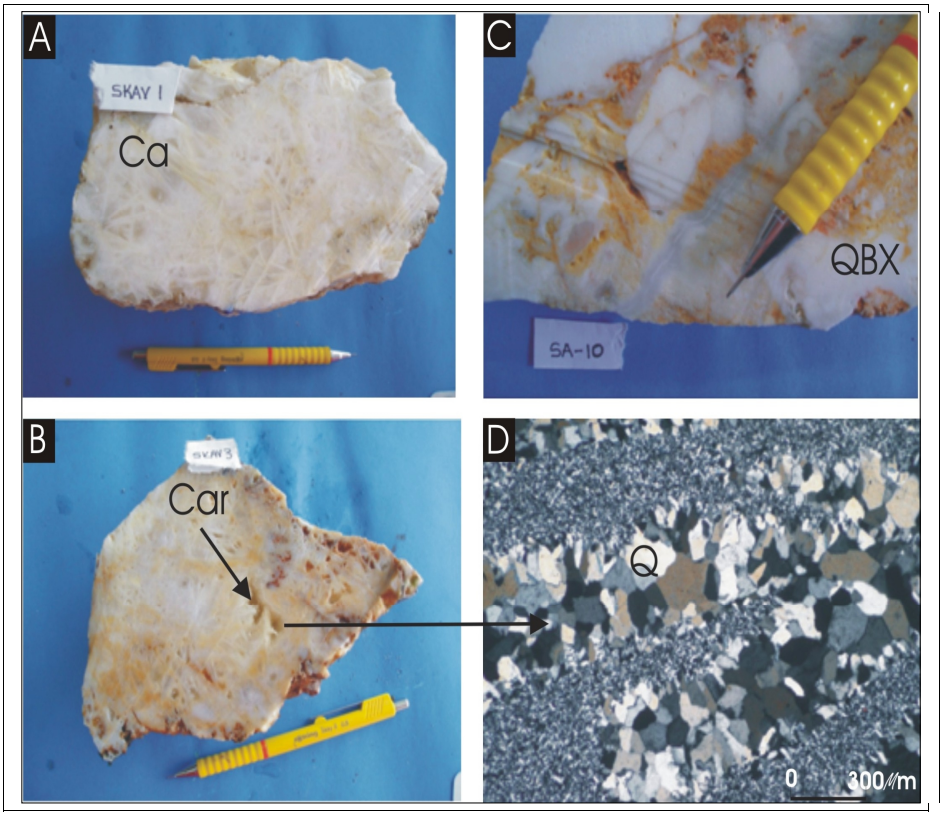

Figure 2.3 Primary epithermal quartz vein textures in the area: A) Typical lattice-bladed carbonate (Ca) replacement texture; B) Coarse-banded chalcedonic quartz vein with bladed carbonate (Car) textures replaced by quartz; C) Quartz breccias (QBX); D) The microscopic image of the coarse-banded chalcedonic quartz vein with bladed carbonate (Car) textures replaced by quartz (Q).

The origin of quartz textures can partly be explained by interpretation of the behavior of quartz, chalcedony and amorphous silica in hydrothermal solutions. As summarized by Fournier (1985a), quartz is the most stable form of silica in hydrothermal systems. Faceted quartz crystals generally grow in solutions which are slightly supersaturated with respect to quartz, indicating relatively slow changing.

Shear planes at quartz are identified. It is shown that the deformation at the environment (Figure 2.4 A). Plagioclase (Figure 2.4 B), amphibol (Figure 2.4 C), biotite (Figure 2.4 E) and the mica (Figure 2.4 F) are identified. All the minerals that are identified shown the host rock is dacite.

Adularia occurs as euhedral rhombs (Figure 2.5 B) either within breccia clasts or as a matrix in veins. The carbonate mineral occurring as infilling vugs (Figure 2.5 D) in the quartz vein is mainly calcite. Stockwork chalcedonic to crystalline quartz in slilicified dacite is common at the area (Figure 2.5 C).

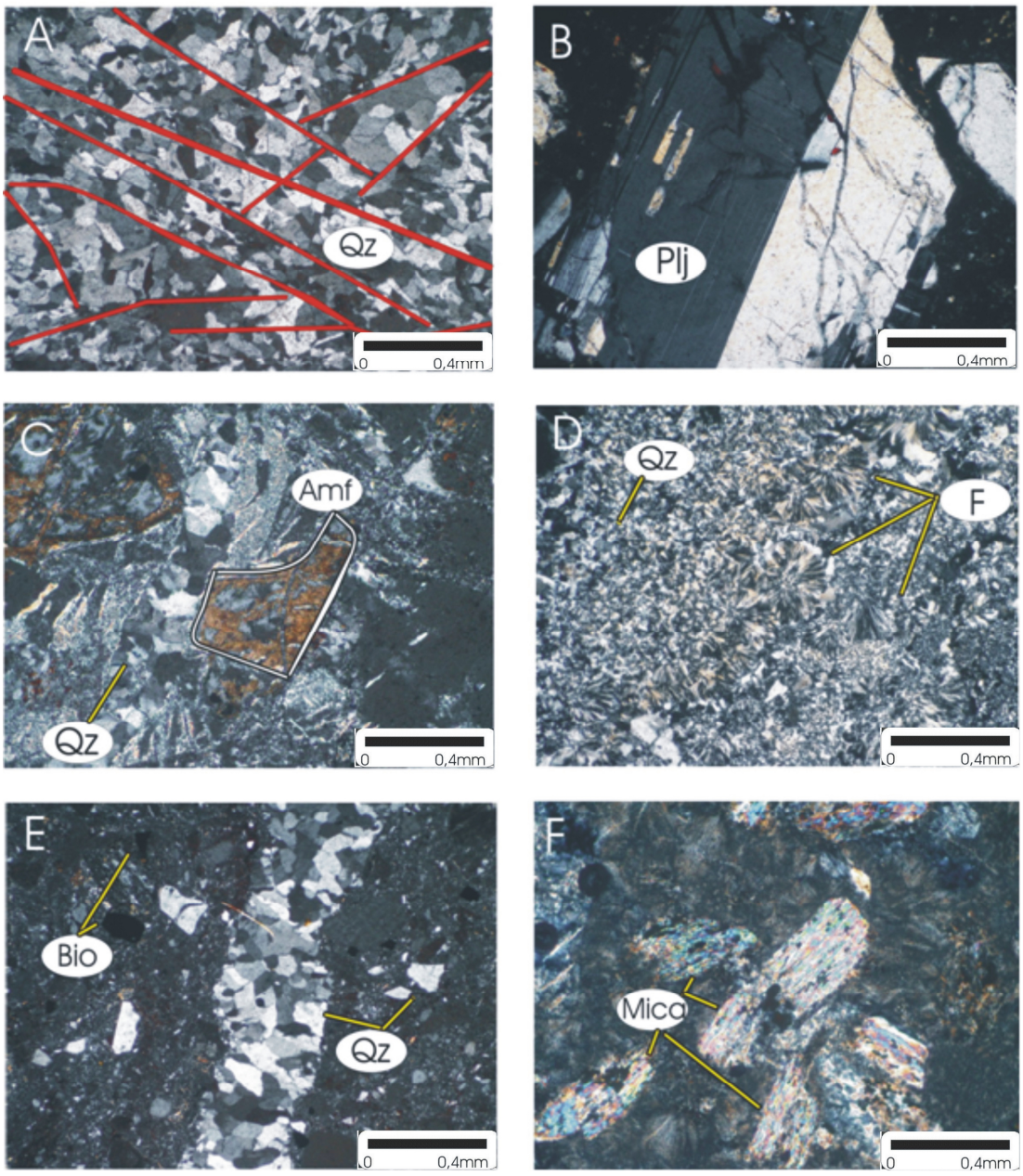

Figure 2.4 Primary epithermal quartz vein textures in the area: A) Shear planes at quartz (Q). B) The plagioclase. C) Amphibol (Amf) and Quartz (Q). D) Feathery (F) appearance in domains within quartz crystals related to formation of crystallites during recrystallization of chalcedony. E) The quartz (Q) with biotite (Bio). F) Biotite partially altered to sericite.

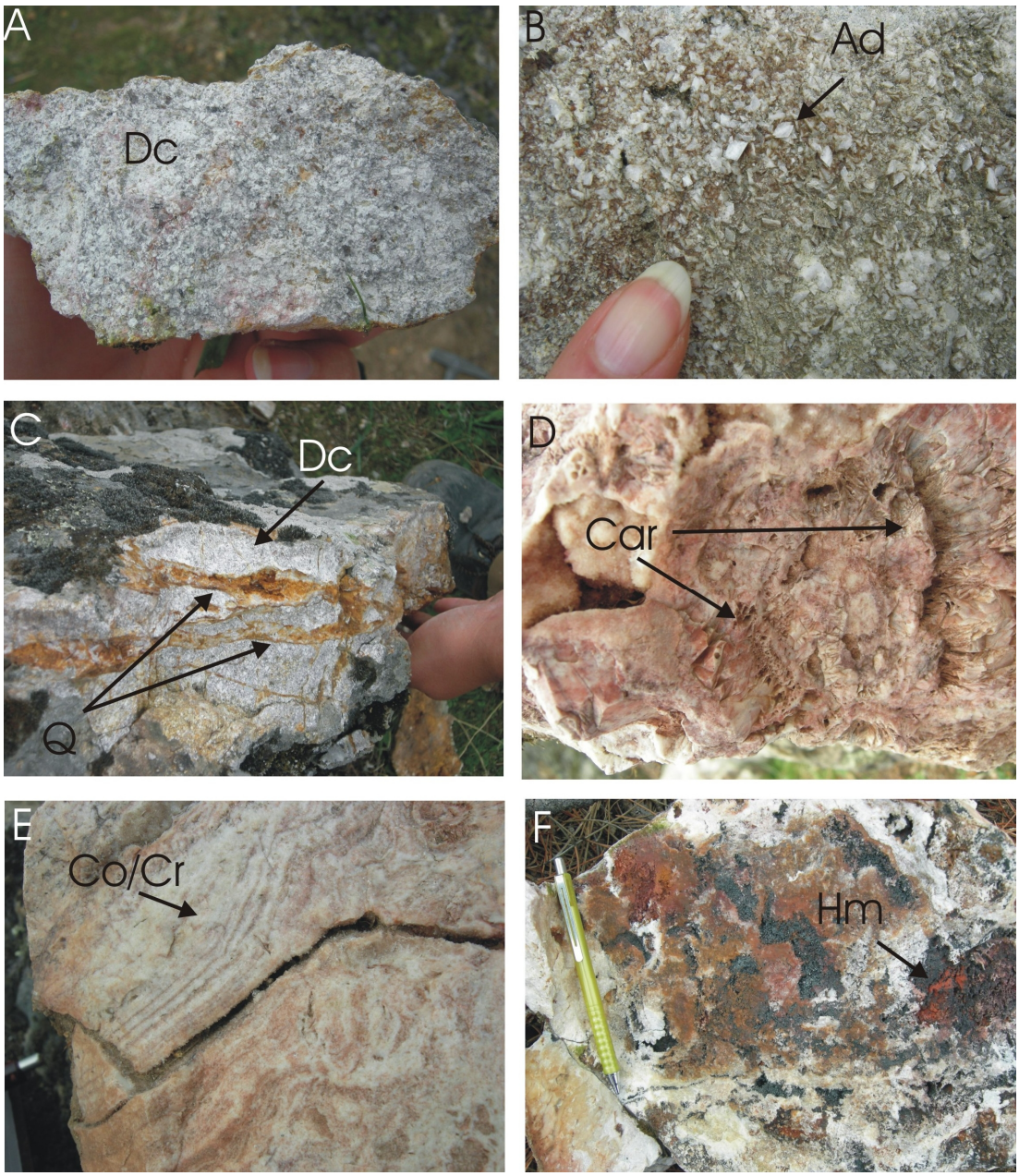

Figure 2.5 A) Hydrothermal altered dacitic (Dc) wall rock sample. B) Adularia (Ad) occurs as euhedral rhombs either within breccia clasts or as a matrix in veins. C) Quartz (Q) stockworks in altered dacitic (Dc) wall rock sample. D) Coarse-banded chalcedonic quartz vein with bladed carbonate (Car) textures replaced by quartz. E) Colloform/crustiform (Co/Cr) banded quartz vein. F) Quartz vein breccia with hematite matrix.

2.2.2 Ore Mineralogy

Pyrite, electrum, gold, silver, argentite; chalcopyrite, sphalerite, galena, tetrahedrite, silver sulphosalt and/or selenide are common minerals in Sindirgi region. However, ore mineral assemblage at Kiziltepe prospect is very simple and consists mainly of electrum, argentite and pyrite (Company reports). Deposits in the whole can be strongly zoned along strike and vertically. They are commonly zoned vertically over 250 to 350 m from a base metal-poor, Au-Ag-rich top to a relatively Ag-rich base metal zone and an underlying base metal-rich zone grading at depth into a sparse base metal, pyritic zone. From surface to depth, metal zones contain: Au-Ag-As-Sb-Hg, Au-Ag-Pb-Zn-Cu and Ag-Pb-Zn within the Sindirgi region (Sindirgi Gold Project, Unpublished company reports). Prospect locations, drill holes locations at Kiziltepe and Kepez sample locations are shown in Figures (2.6-2.7-2.8-2.9-2.10). Sample descriptions are also shown in Table 2.1.

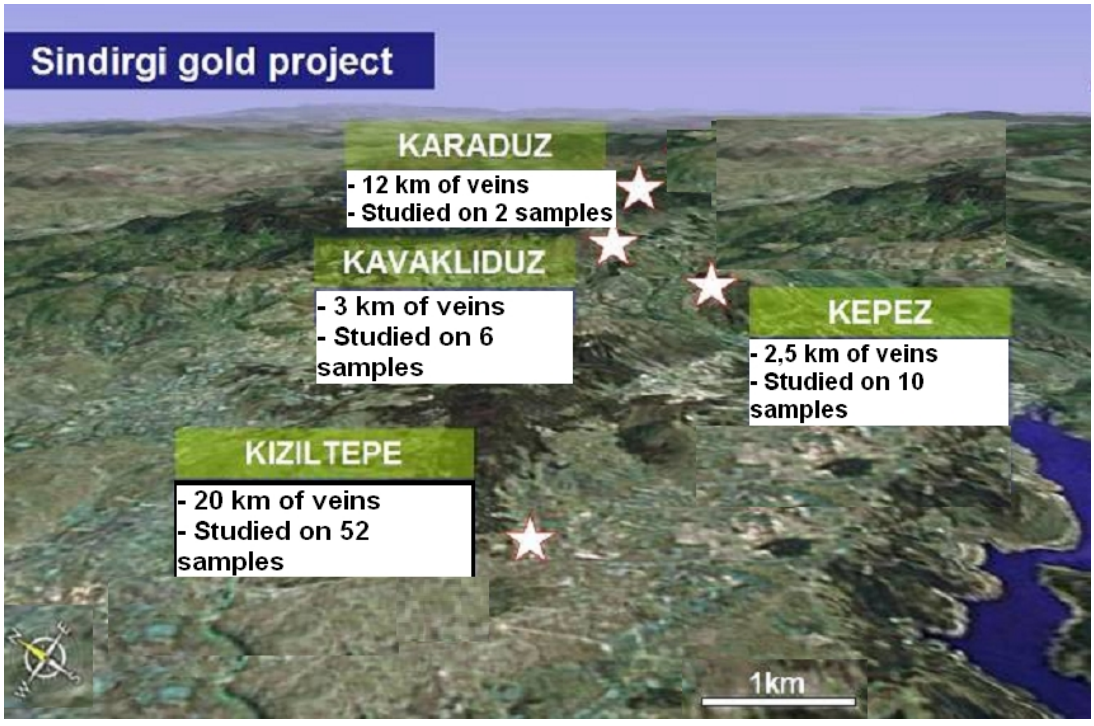

Figure 2.6 Sindirgi gold-project prospect areas.

Table 2.1 Summary of the sample

No	Sample No	Area	Easting	Northing	Thin Section	FI	Ar/Ar Age	Geochem	XRD	Description
1	SA1	Kiziltepe	607896	4348651	x					Crystalline quartz
2	SA2	Kızıltepe	607889	4348663				x	x	Argillic-silisic alteration with stockwork
3	SA3	Kızıltepe	607874	4348670	x			x		Crystalline quartz
4	SA4	Kızıltepe	607818	4348719	x					Crystalline to massive quartz
5	SA5	Kızıltepe	607780	4348749	x	x				Massive crystalline quartz
6	SA6	Kızıltepe	607871	4348695					x	Argillic-silisic alteration
7	SA7	Kızıltepe	607912	4348628	x			x	x	Argillic-silisic alteration
8	SA8	Kızıltepe	607994	4348509	x	x				Lattice bladed,vug in fill textures
9	SA9	Kızıltepe	607169	4349463	x					Lattice bladed,vug in fill textures
10	SA10	Kızıltepe	607166	4349520	x					Lattice bladed,vug in fill textures
11	SA11	Kızıltepe	607114	4349576	x	x				Lattice bladed,vug in fill textures
12	SKAV1	Kavaklıduz	617838	4351683	x	x		x		Crystalline quartz
13	SKAV2	Kavaklıduz	618069	4351800	x				x	Argillic-silisic alteration
14	SKAV3	Kavaklıduz	616193	4351921	x	x				Iron oxide
15	SKAV4	Kavaklıduz	617560	4352154	x					Crystalline quartz
16	SKAV5	Kavaklıduz	617523	4352169	x					Crystalline quartz
17	SKAV6	Kavaklıduz	617281	4352061					x	Argillic-silisic alteration
18	SKAR1	Karadüz	617505	4353721	x	x		x		Crystalline quartz
19	SKAR2	Karadüz	617465	4353691	x					Carbonate replacement

No	Sample No	Area	Easting	Northing	Thin Section	FI	Ar/Ar Age	Geochem	XRD	Description
20	KEP1	Kepez	613801	4351430	x	x		x		Massive crystalline quartz
21	KEP2	Kepez	613799	4351449	x	x				Massive crystalline quartz
22	KEP3	Kepez	613807	4351473	x					Massive crystalline quartz
23	KEP4	Kepez	613791	4351336	x					Vug in fill textures
24	KEP5	Kepez	613791	4351332	x					Crystalline quartz
25	KEP6	Kepez	613761	4351340					x	Argillic-silisic alteration
26	KEP7	Kepez	613719	4351298					x	Argillic-silisic alteration
27	KEP8	Kepez	613964	4350824	x	x				Crystalline quartz
28	KEP9	Kepez	614012	4350394	x					Crystalline quartz
29	KEP10	Kepez	613999	4350357	x					Crystalline quartz
30	FRESH 1-2	Kiziltepe	605595	4349848	x					Dacite
31	C1	Kızıltepe07	608041	4348687	x	x		x		Crystalline quartz
32	C2	Kızıltepe10	608077	4348412	x					Crystalline to massive quartz
33	C3	Kızıltepe13	607089	4349521	x					Massive crystalline quartz
34	C4	Kızıltepe15	606652	4348771	x					With pyrite
35	C5	Kızıltepe16	607234	4349555	x	x				Colloform/crustiform
36	C6	Kızıltepe16	607234	4349555	x					Argillic alteration
37	C7	Kızıltepe16	607234	4349555	x					Crystalline quartz
38	C8	Kızıltepe16	607234	4349555	x					Crystalline quartz

No	Sample No	Area	Easting	Northing	Thin Section	FI	Ar/Ar Age	Geochem	XRD	Description
39	C9	Kızıltepe16	607234	4349555	x					Massive crystalline quartz
40	C10	Kızıltepe18	608134	4348336	x					Massive crystalline quartz
41	C11	Kızıltepe18	608134	4348336	x	x		x		Dacite
42	C12	Kızıltepe18	608134	4348336	x					Lattice texture with quartz
43	C13	Kızıltepe03	607949	4348667	x					Lattice texture with quartz
44	C14	Kızıltepe03	607949	4348667	x					Lattice texture with quartz
45	C15	Kızıltepe03	607949	4348667	x					Lattice texture with quartz
46	C16	Kızıltepe03	607949	4348667	x					Lattice texture with quartz
47	C17	Kızıltepe03	607949	4348667	x					With amesist
48	C18	Kızıltepe03	607949	4348667	x				x	Argillic-silisic alteration
49	C19	Kızıltepe09	608077	4348519	x					Massive crystalline quartz
50	C20	Kızıltepe09	608077	4348519	x					Massive crystalline quartz
51	C21	Kızıltepe09	608077	4348519	x					Massive crystalline quartz
52	C22	Kızıltepe09	608077	4348519	x	x		x		Massive crystalline quartz
53	C23	Kızıltepe04	607867	4348742	x					Lattice texture with quartz
54	C24	Kızıltepe06	607725	4348886	x					Adularia with quartz
55	C25	Kızıltepe06	607725	4348886	x				x	Argillic-silisic alteration
56	C26	Kızıltepe05	607799	4348806	x					Massive crystalline quartz
57	C27	Kızıltepe06	607725	4348886	x					Massive crystalline quartz

No	Sample No	Area	Easting	Northing	Thin Section	FI	Ar/Ar Age	Geochem	XRD	Description
58	C28	Kızıltepe06	607725	4348886	x	x		x		Massive crystalline quartz
59	C29	Kızıltepe06	607725	4348886	x					Massive crystalline quartz
60	C30	Kızıltepe06	607725	4348886	x				x	Argillic-silisic alteration
61	C31	Karadüz01	617638	4353760	x					Massive crystalline quartz
62	C32	Karadüz01	617638	4353760	x					Massive crystalline quartz
63	AKAY YAS 1 (756)	AKAY YAS1	607463	4350786	x		x			Ignimbrite
64	AKAY YAS 2 (817)	AKAY YAS2	609840	4350263	x		x			Ignimbrite
65	YN1ab YN6	KTPD10a06	608011	4348562	x					Crystalline quartz
66	YN2	KTPD5a06	607852	4348743	x					Crystalline quartz
67	YN3ab	KTPD2706	609602	4349673	x					Crystalline quartz
68	YN4ab	KTPD2306	607119	4349498	x		x			Crystalline quartz
69	YN5	KTPD1306	608046	4348375	x		x			Crystalline quartz
70	YN7	KTPD1206	608044	4348432	x					Crystalline quartz

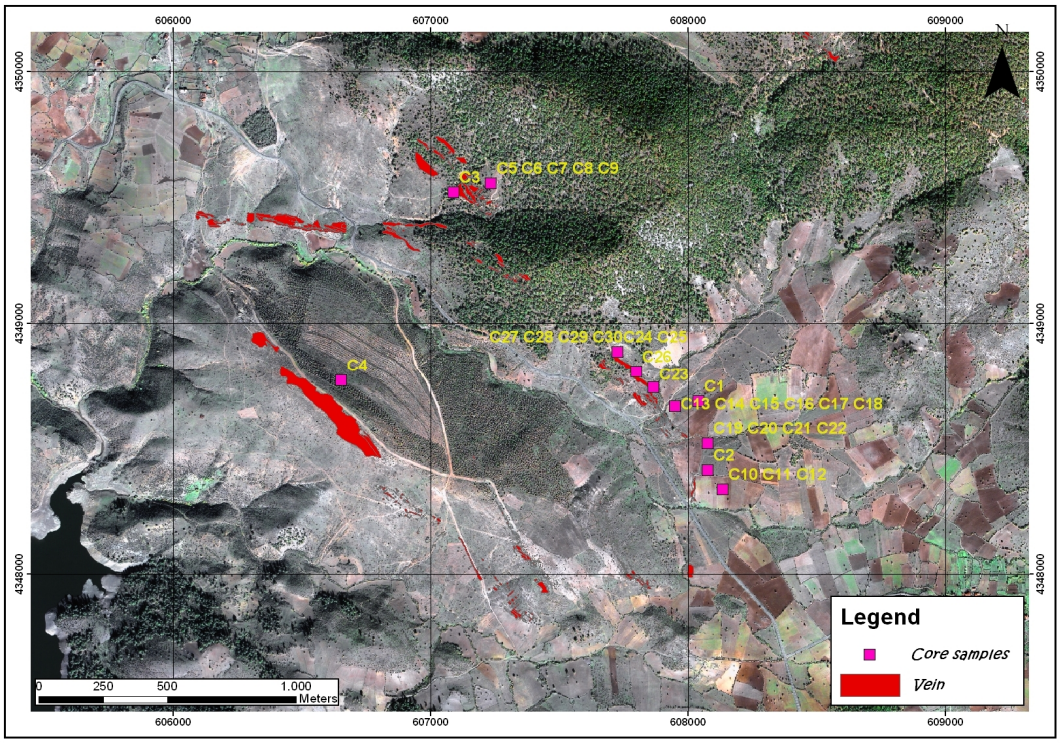

Figure 2.7 Drill holes locations.

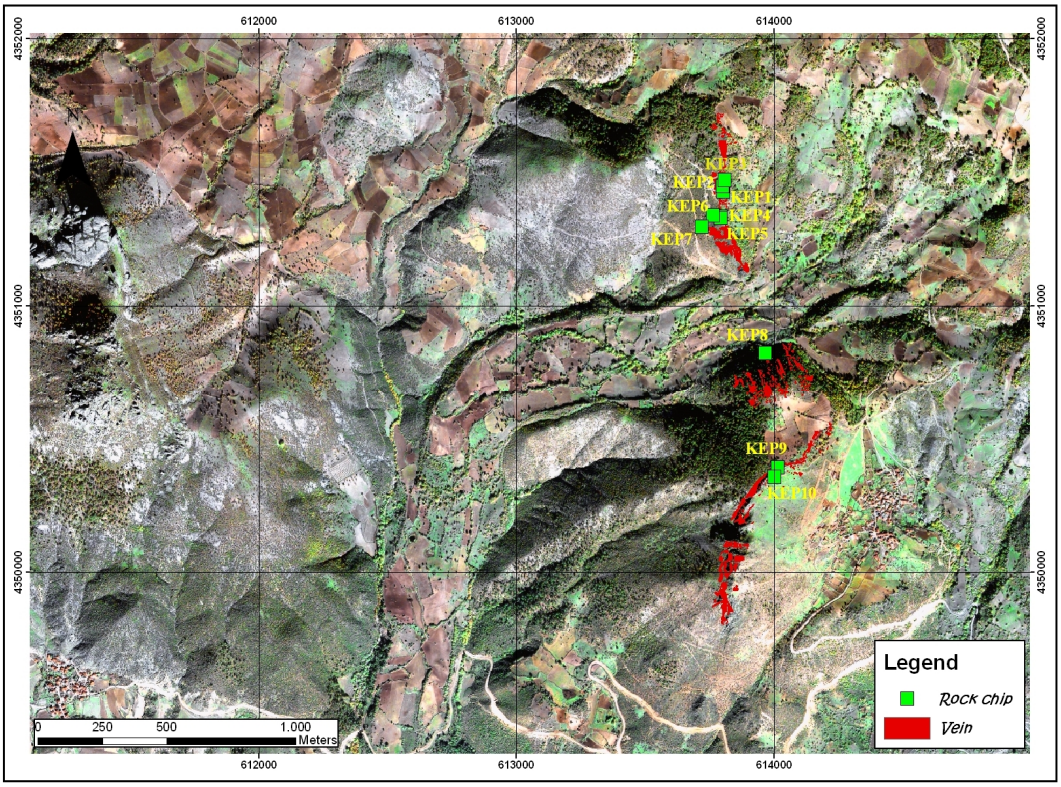

Figure 2.8 The samples of Kepez locations.

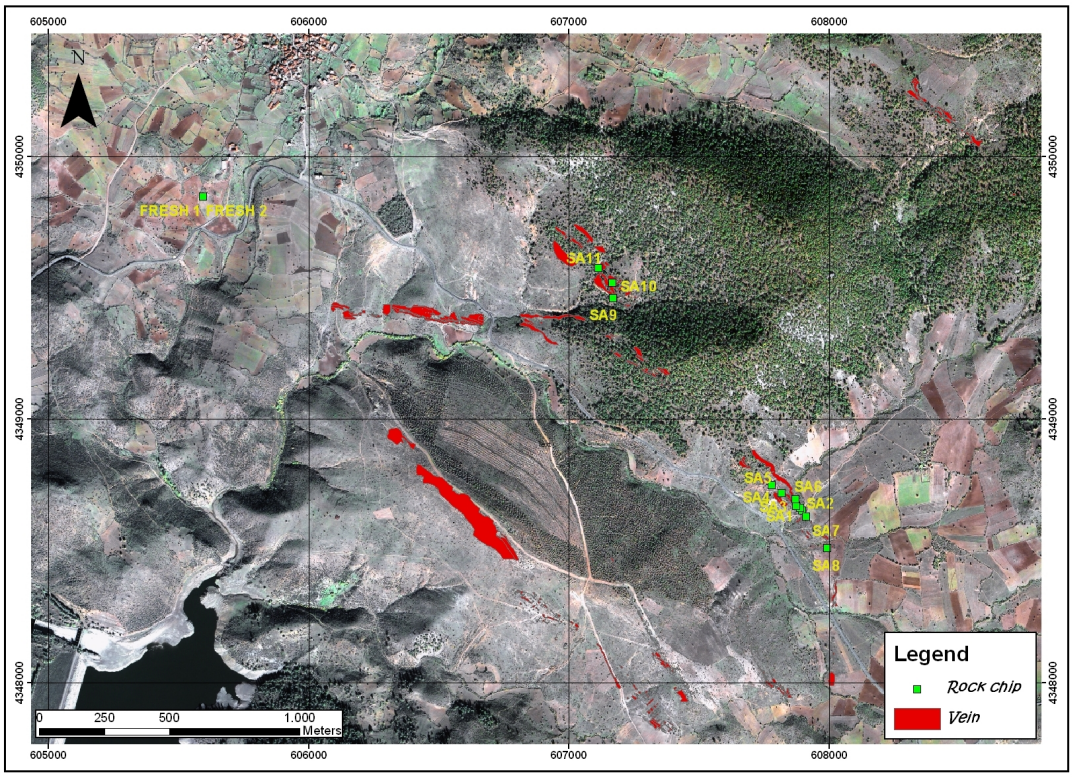

Figure 2.9 Kiziltepe sample locations.

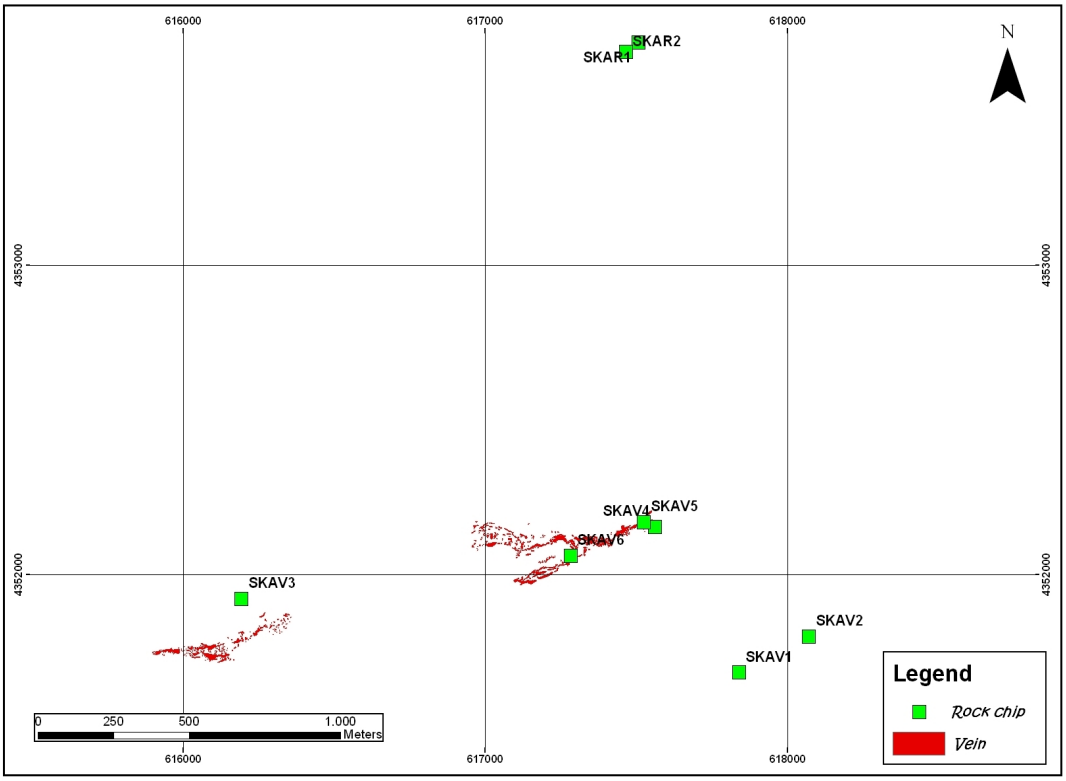

Figure 2.10 Karaduz and Kavakliduz locations.

2.3. Hydrothermal alteration

Interpretation of whole rock X-ray diffraction graphics determined that the main alteration minerals are shown on Table x. In the study area, silicified zones at the center are enveloped by zones of argillic alteration in dacitic ignimbrites, which are in turn encompassed by propylitic alteration consisting mainly of pyrite and chlorite with minor illite and smectite. The argillic zone proximal to major quartz veins is dominated by quartz (quartz is the gangue phase in adularia sericite gold-silver systems (Hayba et al., 1985) + K-Feldspar (adularia) + kaolinite (nacrite) ± illite/smectite (Table 2.2). Argillic alteration is characterized by illite, smectite and kaolinite. Alteration minerals in Kiziltepe areas are similer to those of Kavaklidüz and Kepez areas.

The wall rock alteration assemblages, along with quartz, adularia and calcite include K-mica, chlorite and pyrite. Interstratified illite-smectite and smectite clays plus kaolinite can occur on the margins of the system, where temperatures were cooler and vapor condensates may have been present. Thus, alteration mineralogy shows the characteristics low sulfidation systems. Indirectly forms as a by-product of boiling (Simmons and Browne, 2002). Interpreted clay fractions from X-ray diffractograms are kaolinite, illite, smectite and interstratified illite-smectite. In general, the Kavaklıdüz samples contain minor illite and kaolinite.

Table 2.2 Summary of alteration minerals identified from whole rock and clay separate X-ray diffractogram profiles.

Sample	**Area**	**Minerals identified from XRD diffractogram profiles**
SA 2	Kızıltepe	Quartz(low), K-Feldspar (high), Muscovite, Kaolinite (Nacrite), Smectite
SA 6	Kızıltepe	Quartz(low), K-Feldspar, Kaolinite (Nacrite), Muscovite
SA 7	Kızıltepe	Quartz, K-Feldspar (orthoclase), Kaolinite (Nacrite), Muscovite
C 18	Kızıltepe	Quartz, Kaolinite (Nacrite)
C 25	Kızıltepe	Quartz, K-Feldspar (high), Muscovite, Kaolinite (Dickite)
C 30	Kızıltepe	Quartz, K-Feldspar (high), Muscovite, I-S (55/S), Kaolinite (Nacrite)
SKAV 2	Kavaklıdüz	Quartz, Na-Feldspar, Illıte, Chlorite, Mica (RS), Kaolinite
SKAV 6	Kavaklıdüz	Quartz, K-Feldspar (orthoclase), Kaolinite (Nacrite), Illite
KEP 6	Kepez	Quartz, K-Feldspar [high), Muscovite, Kaolinite (Nacrite)
KEP 7	Kepez	Quartz, K-Feldspar [high), Muscovite, Antigorite, Kaolinite

2.4 Geochemistry

Sampling from altered rocks in this study an ideal opportunity to investigate possible systematic variations in precious and base metals, REE, minor elements and major oxides in hydrothermally altered volcanics (e.g., Bau, 1991; Palacios et al., 1986; Michard, 1989; Terakado and Fujitani, 1998 Bierlein et al., 1999; Bi et al., 2004). Data for all samples are presented in Table 2.3. Fresh volcanic-normalized trace element patterns of wallrock and vein quartz from Karadüz, Kavakliduz, Kiziltepe and Kepez areas (Figures 2.12, 2.13) are also presented. Besides, there are chondrite-normalized patterns (Figure 2.14) and scatter diagrams (Figure 2.15, 2.16).

The degree of leaching is highly variable for major and trace elements. Cs is enriched by a factor of 3 whereas Sr shows 4, Zn shows 9 fold depletions in altered wall rocks (Figure 2.12). Of the major elements, Mg is depleted by a factor of 5.5. Due to structurally-controlled pervasive alteration, Ca and Na are depleted in plagiocalse, and Mg and Fe are depleted in biotite whereas, K, Rb and Cs are enriched in adularia or illite/sericite (Table x and Figure x). Cs and Rb enrichment in the wall rock is caused by replacement of K by these elements in the İllite/sericite. Trace elements such as Ba, Nb, La, Ce, Sr, Nd, Zr, Tb and Y in mineralized quartz veins show 1 to 3 fold depletions. In other words, Th and Sr along with La, Ce, Nd, Zr, Tb and Y elements show moderate depletions in quartz veins (Figure 2.12, 2.13). The average concentration of Mg, Fe, Na and Ca is also very low (Table 2.3). All rare earth elements (REE) in altered wall rock LREE (La-Eu) concentrations in quartz veins are lower than in the host volcanic rocks. A linear trend from Gd through Tb, Ho to Yb occurs and their contents appear to be reduced by a factor of not more than 1.5.

Figure 2.12 and 2.13 represents a mixture of normalized minor elements and REE profiles of altere volcanics and quartz veins in Karadüz, Kavaklidüz, Kiziltepe and Kepez. Also presedent in Figure 2.14 is chondrite-normalized REE-profiles of the

above mentioned rocks. From the altered volcanics to quartz veins, there is a further depletion of total REE, indicating progressive leaching of the REE with increasing fluid/rock ratios and decrease in pH. The mobilization of REE, including either depletion or enrichment, occurs under conditions of large-scale fluid flow (Pirajno, 1995).

Geochemical relationship between Au-Ag and associated elements from mineralized epithermal quartz veins are presented in Table x and Figure x and x. Positive correlation coefficients of Au with Ag and Sb in epithermal quartz veins are strong, all of which greater than 0,50. Correlations between Au-As and Au-Cu are very weak whereas no correlation occurs between Ag and Cd. All these indicate that there may be different mineralizing event there by possible introduction of Au and Ag different phases of mineralization.

There are very strong correlation coefficients of Ag with Au (R=0,93) and Sb (R=0,79) which suggested that all of these elements are related to the same mineralizing event(s).

Negative correlation coefficients between SiO_2 and REE (Table 2.4) and positive correlations coefficients between K and REE are very strong. Although there appears to be very strong correlation coefficients among Ba, Rb,Sr and REE, no correlations are appear between SiO_2 and Au, Ag and Sb (Table 2.4).

Correlation coefficients between Au and Ag is very strong (R=0,96) (Table 2.4). It is important to consider that Ag/Au ratio is 10. Galata assay results returned a Ag/Au ratio of 22 from 2500 core samples. This ratio is important as an exploration guide in establishing the nature of the system as well as elucidating metal enrichment and zoning (Cole and Drummond, 1986). If epithermal systems with Ag/Au ratios (as is the case of study area) are ~1, they contain mainly electrum and free gold. Au - thisulfide complex is dominant and the temperature of formation is less than 250 °C.

Table 2.3 Major and geochemistry results

Samples	***SiO2***	***Al2O3***	***Fe2O3***	***MgO***	***CaO***	***Na2O***	***K2O***	***TiO2***	***P2O5***	***MnO***	***Cr2O3***	***Ni***	***Sc***	***LOI***
	%	%	%	ppm	ppm	ppm	ppm	ppm	%	%	ppm	ppm	ppm	%
KEP 1	97,97	0,52	0,77	200	800	200	500	100	0,02	100	30	15	1	0,6
SKAV 1	71,48	0,47	0,42	1100	152300	300	600	100	0,02	500	10	17	1	12,0
SKAR 1	96,73	1,08	1,15	100	200	100	1100	300	0,01	100	10	12	1	0,9
SA 2	69,62	15,06	2,66	3000	1500	3000	71100	5600	0,06	100	20	11	10	3,9
SA 3	96,15	0,71	1,61	100	400	300	2100	100	0,05	100	20	5	1	1,1
SA 7	75,4	10,93	2,99	900	800	2100	58900	4100	0,14	100	10	10	7	3,6
C 1	97,66	0,67	0,77	200	200	300	800	100	0,01	100	20	11	1	0,8
C 11	88,02	5,39	1,91	1900	1300	300	13600	1700	0,09	200	10	13	3	2,6
C 22	97,8	0,73	0,62	100	200	100	500	100	0,02	100	10	7	1	0,8
C 28	98,17	0,35	0,65	100	200	100	400	100	0,01	100	10	5	1	0,8
753 (Fresh ignimbrite, FI)	66,02	15,32	4,18	15600	31700	32400	35550	5600	0,18	800	20	5	9	2,0

Samples	***Ba***	***Be***	***Co***	***Cs***	***Ga***	***Hf***	***Nb***	***Rb***	***Sn***	***Sr***	***Ta***	***Th***
	ppm	ppm	ppm	ppm	ppm	ppm	ppm	ppm	ppm	ppm	ppb	ppm
KEP 1	33	2	0,5	2	3,2	0,5	0,5	4	1	19	0,1	0,2
SKAV 1	15	3	0,5	1,5	0,8	0,5	0,5	4	1	845	0,1	0,1
SKAR 1	25	5	0,7	0,6	12,9	0,5	1,1	8	1	5	0,1	1,7
SA 2	1278	2	2,3	8,6	16,5	6,1	14,5	268	3	100	1,1	15,9
SA 3	83	3	0,6	2	6,6	0,5	0,5	9	1	31	0,1	0,4
SA 7	1133	2	0,6	4,9	9,6	4,3	10,2	190	3	155	0,9	13,9
C 1	20	1	1,5	1,5	3,9	0,5	0,5	4	1	17	0,1	0,2
C 11	114	2	3,2	4	6,4	1,9	4,3	55	1	24	0,3	5
C 22	21	2	0,6	1,3	1,4	0,5	0,5	3	1	40	0,1	0,1
C 28	8	2	0,7	0,8	3,9	0,5	0,5	2	1	14	0,1	0,1
753 (Fresh ignimbrite, FI)	1132	3	7,6	3,1	18,1	5,6	14,7	134	3	388	1,2	19,4

Samples	***U***	***V***	***W***	***Zr***	**Y**	***La***	***Ce***	***Pr***	***Nd***	***Sm***	***Eu***	***Gd***
	ppm	ppm	ppm	ppm	ppm	ppm	ppm	ppm	ppm	ppm	ppb	ppm
KEP 1	0,1	5	0,2	2	0,3	0,4	1,1	0,15	0,4	0,05	0,02	0,09
SKAV 1	0,1	5	1,9	1	1	0,5	0,7	0,11	0,3	0,06	0,03	0,19
SKAR 1	0,4	6	0,5	14	1,6	1,7	3,8	0,47	1,6	0,31	0,07	0,39
SA 2	4,1	60	19,6	205	24	37,5	67	7,14	23,3	4,22	1,23	3,46
SA 3	0,4	5	13,8	4	1	1,5	2,7	0,34	1,1	0,17	0,03	0,27
SA 7	3,3	38	13,9	146	14,6	31,6	62,5	7,16	25,7	3,57	0,8	2,59
C 1	0,1	5	3,8	5	0,4	0,6	1,1	0,12	0,3	0,05	0,02	0,11
C 11	2,4	54	1,8	58	13,6	13,4	25,1	2,85	10,7	2,05	0,68	2,15
C 22	0,1	5	3	2	0,2	0,1	0,4	0,03	0,3	0,05	0,02	0,05
C 28	0,1	5	0,2	2	0,2	0,1	0,3	0,04	0,3	0,05	0,02	0,05
753 (Fresh ignimbrite, FI)	5	73	1,5	200	26,8	48,1	87,7	9,66	34	5,66	1,13	4,65

Samples	*Tb*	*Dy*	*Ho*	*Er*	*Tm*	*Yb*	*Lu*	*Mo*	*Cu*	*Pb*	*Zn*	*Ni*
	ppm	ppm	ppm	ppm	ppm	ppm	ppm	ppm	ppm	ppm	ppm	ppm
KEP 1	0,02	0,05	0,02	0,03	0,01	0,05	0,01	4,1	3,0	1,6	2	6,1
SKAV 1	0,03	0,09	0,03	0,06	0,02	0,05	0,01	0,3	1,6	0,5	2	1,2
SKAR 1	0,06	0,29	0,06	0,16	0,05	0,19	0,04	0,8	2,5	2,0	1	2,6
SA 2	0,68	3,86	0,74	2,1	0,35	2,17	0,34	0,3	2,8	22,1	6	2,4
SA 3	0,04	0,16	0,03	0,11	0,02	0,07	0,02	2,0	4,2	3,1	9	3,0
SA 7	0,47	2,42	0,46	1,35	0,22	1,44	0,23	0,6	3,6	20,2	4	1,6
C 1	0,02	0,05	0,02	0,04	0,01	0,06	0,01	0,6	5,0	0,6	1	3,0
C 11	0,41	2,1	0,42	1,09	0,17	1,03	0,15	0,8	2,5	12,5	14	3,1
C 22	0,01	0,05	0,02	0,03	0,01	0,05	0,01	0,7	7,4	1,7	2	2,8
C 28	0,01	0,05	0,02	0,03	0,01	0,05	0,01	0,5	2,1	0,6	1	1,4
753 (Fresh ignimbrite, FI)	0,87	4,27	0,87	2,49	0,38	2,28	0,39	0,8	5,3	13,2	53	4,5

Samples	*As*	*Cd*	*Sb*	*Bi*	*Ag*	*Au*	*Hg*	*Tl*	*Se*
	ppm	ppm	ppm	ppm	ppm	ppb	ppm	ppm	ppm
KEP 1	5,2	0,1	14,0	0,1	48,1	14278	0,10	0,1	1,1
SKAV 1	0,9	0,1	0,3	0,1	0,3	98	0,01	0,1	0,5
SKAR 1	58,1	0,1	9,6	0,1	0,3	60	0,06	0,1	0,5
SA 2	56,1	0,1	3,0	0,1	0,6	12	0,16	0,3	0,5
SA 3	86,9	0,1	3,9	0,1	14,1	985	0,01	0,4	0,5
SA 7	97,2	0,1	2,4	0,1	0,6	126	0,02	0,4	0,5
C 1	2,2	0,1	0,3	0,1	1,8	28	0,01	0,1	0,5
C 11	34	0,1	0,3	0,1	0,8	22	0,01	0,1	0,5
C 22	2,2	0,1	7,7	0,1	100	1458	0,01	0,1	2,3
C 28	11,1	0,1	1,7	0,1	2,3	184	0,03	0,1	0,5
753 (Fresh ignimbrite, FI)	4,8	0,1	0,1	0,1	0,3	7	0,01	0,1	0,5

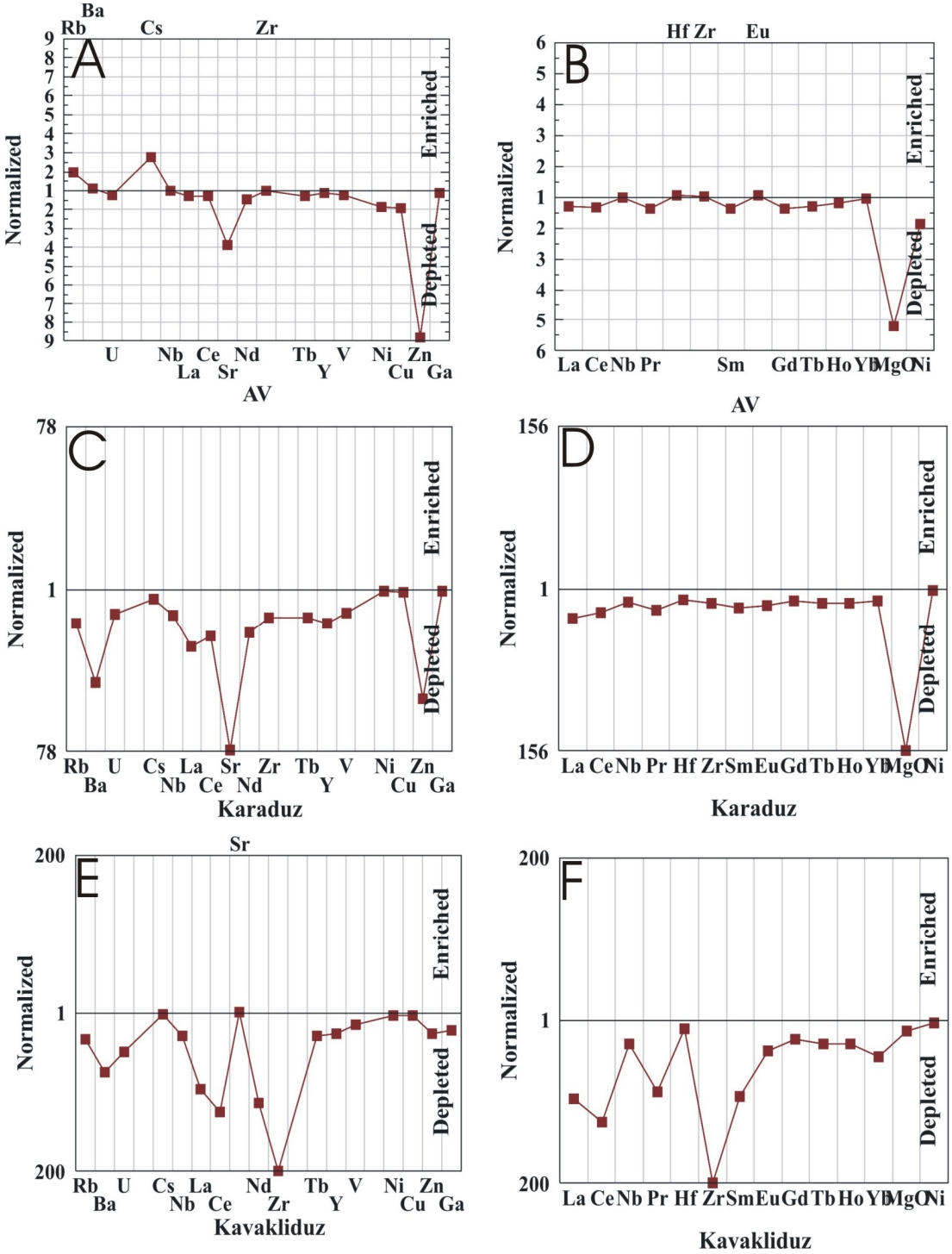

Figure 2.11 Plot of (A) major and trace elements and (B) REE in altered wall rock at Sindirgi prospects; and plot of major –trace and REE at C, D) Karaduz and E, F) Kavakli Duz Prospects normalized against fresh ignimbrite.

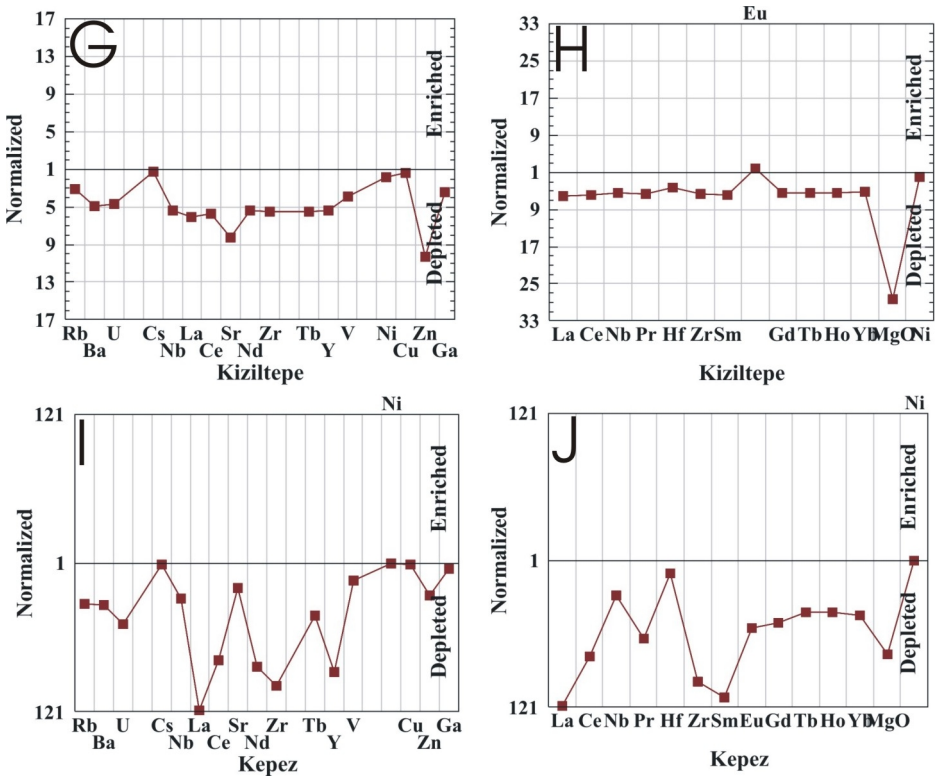

Figure 2.12 Plot of major and trace elements and REE in altered wall rock at G, H) Kiziltepe and I, J) Kepez Prospects, normalized against fresh ignimbrite.

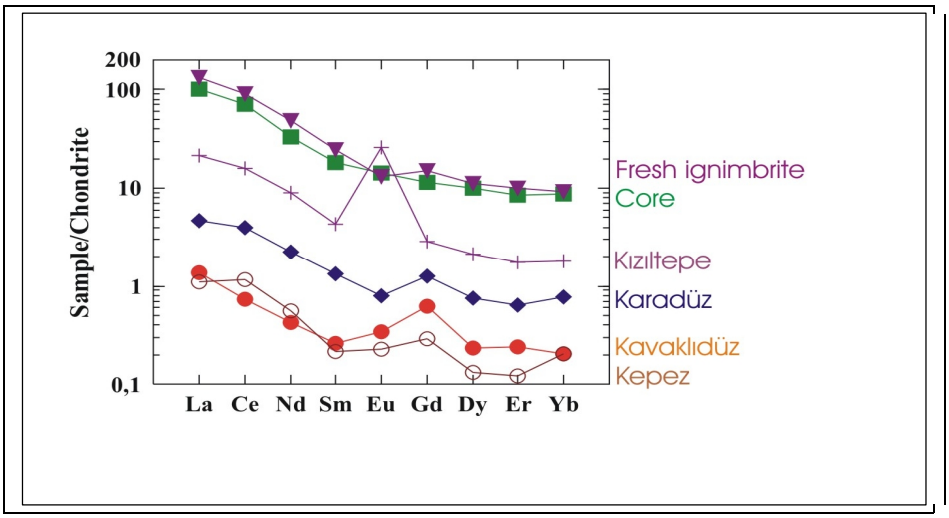

Figure 2.13 Plot of chondrite-normalized REE concentration altered wall rock and quartz veins

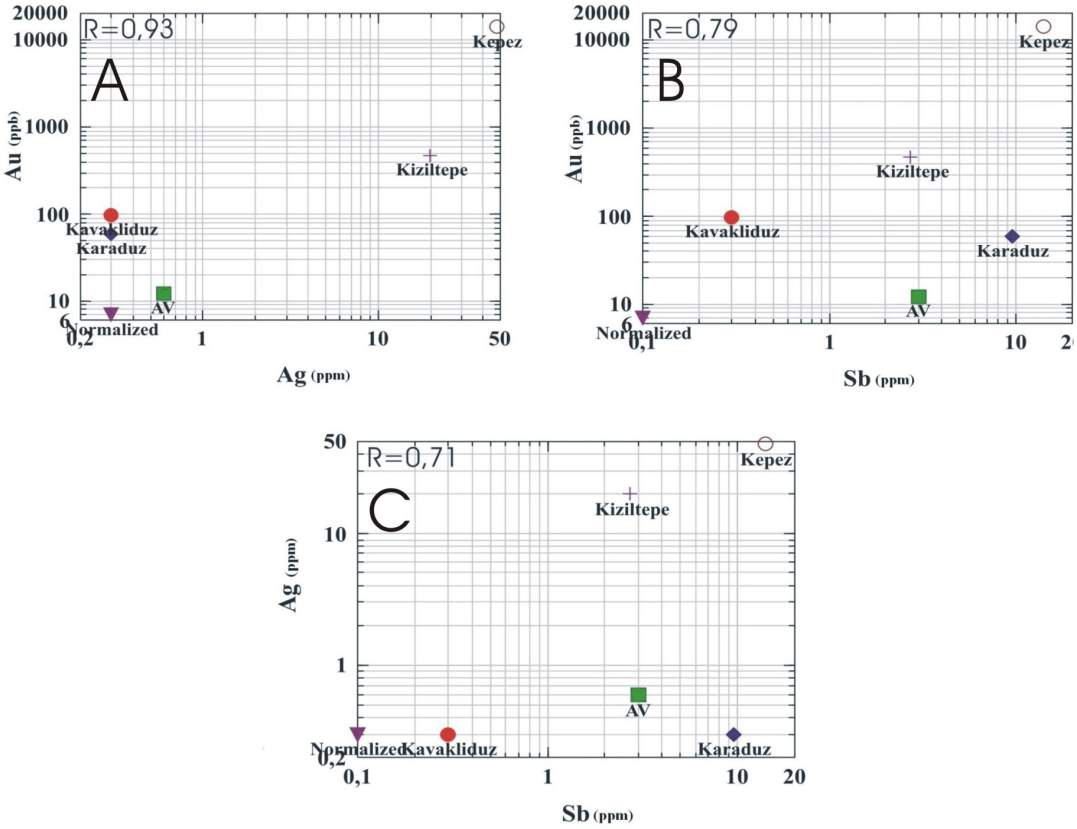

Figure 2.14 Log-Log plot of concentrations of A) Au-Ag, B) Au-Sb and C) Ag-Sb in samples from the study area.

Table 2.4 Matrix of correlations between measured variable for Sindirgi prospects deposits rockchip data set

	Au	Ag	Cu	Pb	Zn	As	Sb	Hg	Mo	Ba	Rb	Sr	Ga	Ta	Nb	K2O	SiO2	MgO	CaO
Na2O	-0,23	-0,31	0,78	0,4	1	-0,37	-0,45	-0,35	-0,16	0,63	0,34	0,21	0,62	0,73	0,7	0,76	-0,59	1	-0,02
CaO	-0,25	-0,35	-0,46	-0,34	-0,03	-0,57	-0,51	-0,49	-0,34	-0,24	-0,28	0,97	-0,47	-0,21	-0,23	-0,25	-0,49	0,01	
MgO	-0,27	-0,36	0,75	0,47	0,99	-0,36	-0,5	-0,3	-0,22	0,69	0,42	0,25	0,65	0,78	0,75	0,77	-0,66		
SiO2	0,53	0,65	-0,16	-0,61	-0,57	0,25	0,82	0,07	0,6	-0,73	-0,64	-0,65	-0,42	-0,75	-0,74	-0,45			
K2O	-0,4	-0,24	0,91	0,57	0,79	-0,05	-0,6	-0,31	-0,32	0,66	0,47	-0,05	0,54	0,72	0,69				
Nb	-0,38	-0,44	0,55	0,93	0,69	0,14	-0,5	0,29	-0,38	1	0,91	-0,02	0,84	1					
Ta	-0,37	-0,43	0,59	0,91	0,73	0,08	-0,52	0,24	-0,36	0,99	0,89	0	0,82						
Ga	-0,43	-0,53	0,51	0,76	0,61	0,44	-0,23	0,28	-0,38	0,81	0,73	-0,29							
Sr	-0,33	-0,43	-0,26	-0,19	0,21	-0,63	-0,64	-0,53	-0,4	-0,04	-0,13								
Rb	-0,35	-0,39	0,28	0,99	0,34	0,37	-0,41	0,57	-0,39	0,94									
Ba	-0,36	-0,42	0,51	0,96	0,63	0,17	-0,49	0,35	-0,37										
Mo	0,99	0,94	0,04	-0,39	-0,17	-0,38	0,81	0,24											
Hg	0,31	0,2	-0,28	0,52	-0,37	0,49	0,43												
Sb	0,79	0,71	-0,25	-0,42	-0,47	0,12													
As	-0,4	-0,31	-0,13	0,37	-0,38														
Zn	-0,24	-0,29	0,81	0,4															
Pb	-0,36	-0,37	0,39																
Cu	-0,08	0,06																	
Ag	0,93																		

2.5 Fluid Inclusion Studies

Fluid inclusion doubly polished sections were prepared for ten samples. For this study, doubly polished quartz wafers approximately 0,2–0,3 mm thick, were prepared from the surface and the core samples. Besides, normal polished thin sections were made from the same samples for microscopic studies (Table 2.5). The polish sections were prepared using Struers RotoPol_35 in Dokuz Eylül University Fluid Inclusion Laboratory (Figure 2.15).

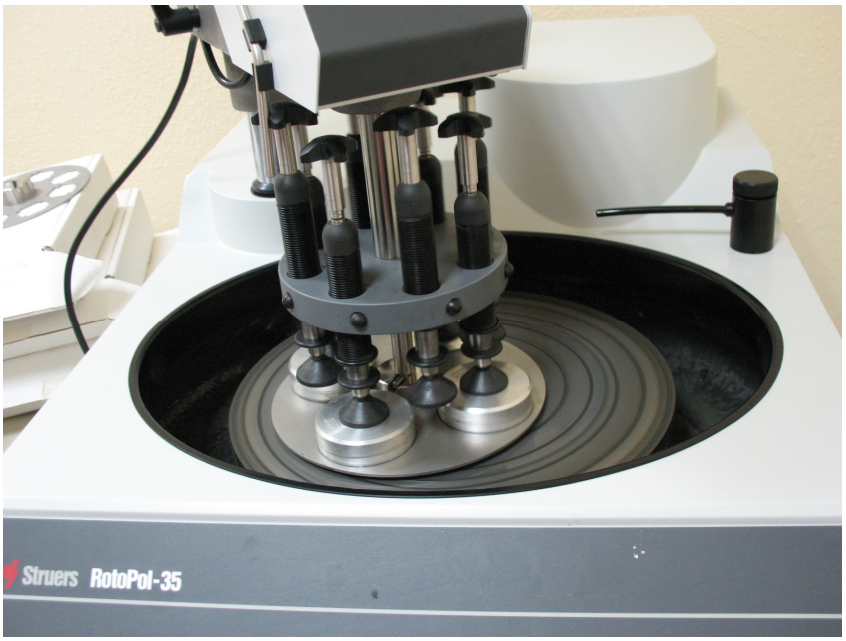

Figure 2.15 Polish section lab for fluid inclusion study in Geology Department at at Dokuz Eylul University.

Heating and freezing measurement were performed on a USGS gas-flow heating/freezing system mounted on a Lincom-600 microscope at the Department of Geology, Dokuz Eylul University, Turkey. The stage was calibrated doing measurements between -190ºC and + 600ºC. Each measurement was repeated three times and was recorded as an average of the three. Photographs of the fluid inclusions were taken prior to microthermometric study in order to record the original vapor and fluid ratio for comparison with those which underwent heating and freezing processes.

During the study, fluid inclusion volumes were calculated from the bubble diameter and the homogenization temperature (Th°C) and fluid compositions were defined by the freezing temperature (Tm_{ice}) and % NaCl equivalent salinity. A total of 178 measurements were done from ten samples (Table 2.5). All the fluid inclusions contained liquid (L) and vapor (V) indicating occurrence of two phases.

Fluid inclusion plates consist of quartz vein material or quartz. The quartz is generally massive chalcedonic to crystalline quartz. Most of the samples that were chosen for fluid inclusion study have two types of inclusions: 1) One phase-vapor, V, inclusions (Figure2.16A). 2) Two-phase liquid-rich, L-V, inclusions (Figure 2.16B). Two-phase liquid rich inclusions are extremely rare with 3 to 8 inclusions seen in any given sample (Figure 2.16C). In every case, the two-phase liquid-rich inclusions show highly variable amounts of vapor and liquid (Figure 2.17).

Ratio of vapor to liquid is highly variable from one fluid inclusion to another in same sample indicating boiling conditions.

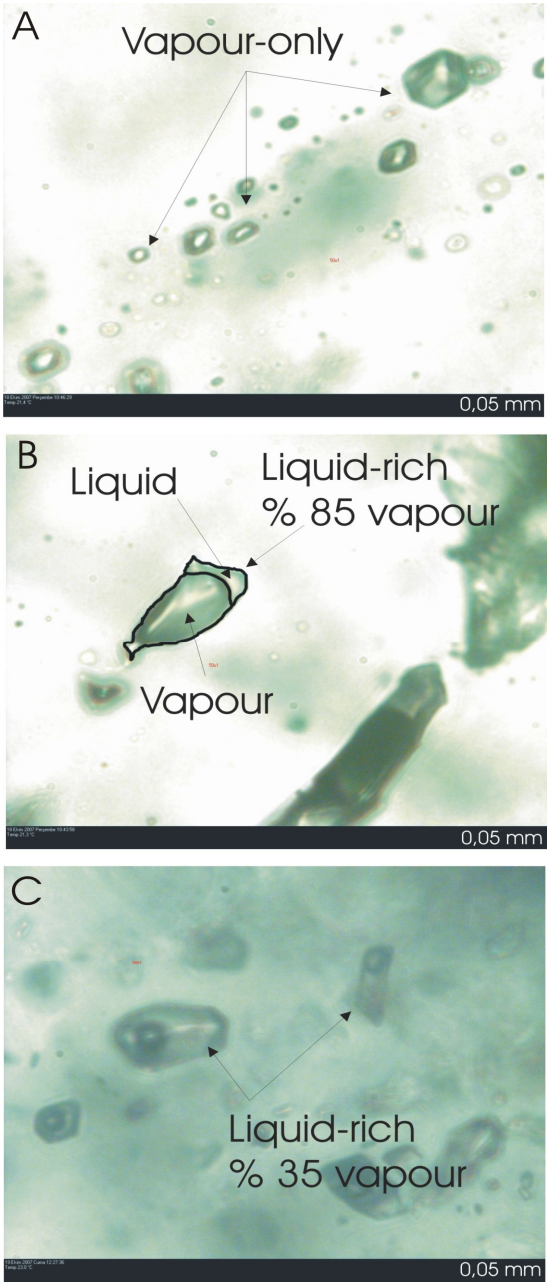

Figure 2.16 Images of fluid inclusions in quartz from core sample (Kiziltepe). A) Single-phase vapor-phase fluid inclusions forming a linear array. B) Two-phase liquid-rich inclusions with variable liquid to vapor ratios (%85 vapor). C) Two-phase liquid-rich inclusions with variable liquid to vapor ratios (%35 vapor).

The fluid inclusions were confirmed were abrupt freezing from 25, 4 °C (room temperature) to –22,5°C. At this time, when the liquid were frozen, the bubble became smaller (Figure 2.17B). At –5 °C, when the ice in the liquid has been crystallized, the bubble became bigger than former and become more circular in shape (Figure 2.17C). At –1.4°C, when the little crystals have disappeared, the bubble still continued to grow (Figure 2.17D). The temperature at which the bubble disappears is called freezing point (Tm $_{ice}$). After defining the Tm $_{ice}$ value, the heating started. At 185,2 °C, the bubble began to shrink and the finally the temperature that the bubble was disappeared is called homogenization temperature (Th°C).

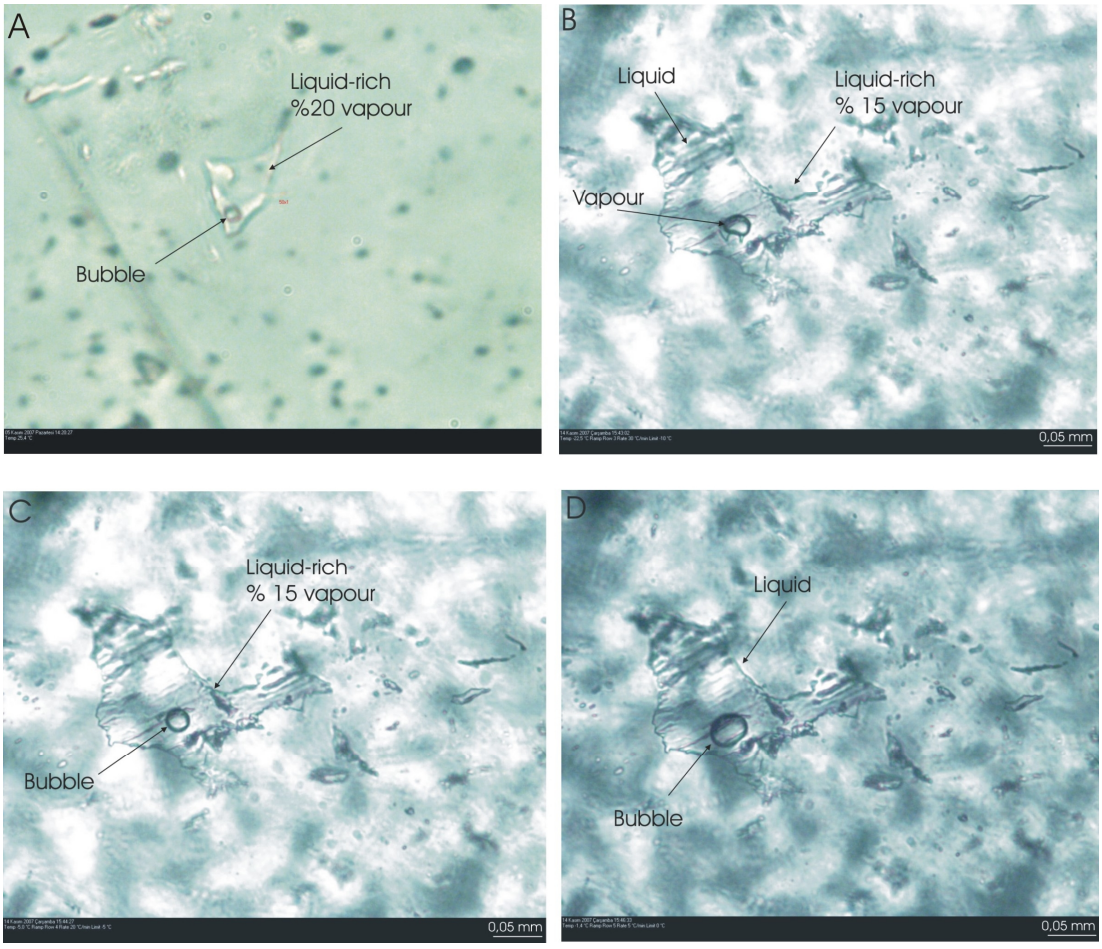

Figure 2.17 Images of freezing experiment on fluid inclusion in quartz A) Liquid-rich % 20 vapor at the room temperature (25,4°C). B) Liquid-rich % 15 vapor at (–22,5°C). C) Liquid-rich % 15 vapor at (-5°C). D) Liquid at (-1,4°C).

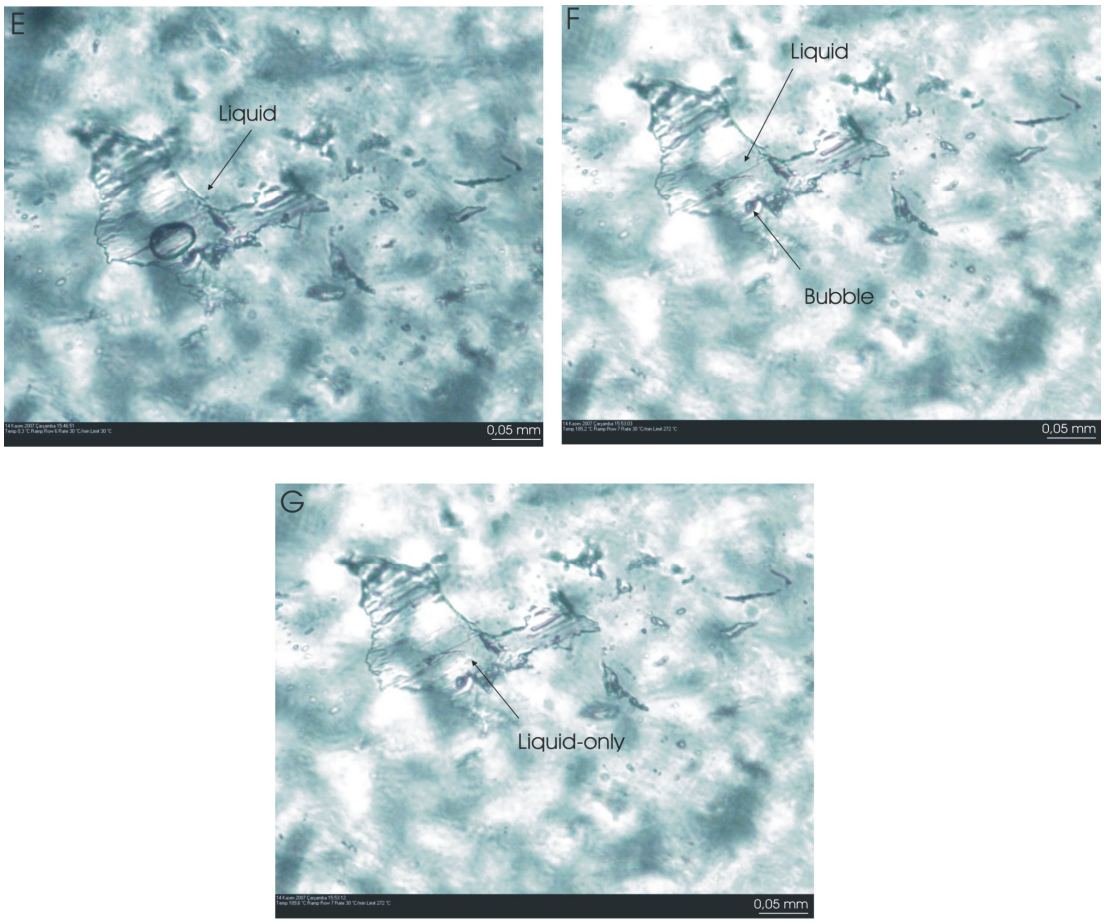

Figure 2.18 Images freezing experiment on fluid inclusion in quartz E) Liquid-rich with the vapor bubble (0,3°C). F) Liquid-rich with the smaller vapor bubble at (185,2°C). G) Completely liquid vapor at (189,6°C).

During the study, the homogenization temperatures (Th°C) and the freezing point (Tm_{ice}) were measured from the fluid inclusions. % NaCl calculated to use from the freezing point values (Table 2.5).

Table 2.5 Data summary on fluid inclusions in the Sindirgi prospect.

Sample	Area	Core Sample	Surface Sample	Depth (m)	Height (m)	Primer	Sec.	Th°C	Tmice	%NaCl Equiv.
C1	Kızıltepe	X		36		X		376	-2	2,6
C1	Kızıltepe	X		36		X		402	-2	2,9
C1	Kızıltepe	X		36		X		335	-2	2,6
C1	Kızıltepe	X		36		X		300	-1	2,4
C1	Kızıltepe	X		36		X		363	-2	3,4
C1	Kızıltepe	X		36		X		366	-2	3,4
C1	Kızıltepe	X		36		X		365	-2	3,4
C1	Kızıltepe	X		36		X		169	-1	1,2
C1	Kızıltepe	X		36		X		239	-0	0,7
C1	Kızıltepe	X		36		X		180	-1	1,2
C1	Kızıltepe	X		36		X		190	-1	1,6
C1	Kızıltepe	X		36		X		169	-1	1,6
C1	Kızıltepe	X		36		X		196	-1	1,6
C1	Kızıltepe	X		36		X		264	-1	2,1
C1	Kızıltepe	X		36		X		193	-1	2,1
C1	Kızıltepe	X		36		X		306	-1	1,1
C1	Kızıltepe	X		36		X		205	-1	2,4
C1	Kızıltepe	X		36		X		243	-1	0,9
C1	Kızıltepe	X		36		X		363	-1	2,1
C1	Kızıltepe	X		36		X		354	-1	1,7
C1	Kızıltepe	X		36		X		392	-1	2,4
C1	Kızıltepe	X		36			X	193	-0	0,5
C1	Kızıltepe	X		36			X	222	-0	0,5
C1	Kızıltepe	X		36			X	230	-1	0,9
C1	Kızıltepe	X		36		X		376	-1	1,1
C1	Kızıltepe	X		36			X	196	-0	0,7
C1	Kızıltepe	X		36		X		236	-1	0,9
C1	Kızıltepe	X		36		X		217	-1	1,1
C1	Kızıltepe	X		36		X		202	-1	1,2
C1	Kızıltepe	X		36		X		326	-0	0,7
C1	Kızıltepe	X		36		X		330	-1	0,9
C1	Kızıltepe	X		36		X		315	-1	0,9
C1	Kızıltepe	X		36		X		265	-1	0,9
C5	Kızıltepe	X		28		X		180	-1	1,2
C5	Kızıltepe	X		28		X		291	-1	0,9
C5	Kızıltepe	X		28		X		286	-0	0,7

C5	Kızıltepe	X		28		X		280	-0	0,4
C5	Kızıltepe	X		28		X		209	-0	0,7
C5	Kızıltepe	X		28		X		218	-0	0,7
C5	Kızıltepe	X		28		X		160	-1	1,1
C5	Kızıltepe	X		28		X		305	-2	2,6
C5	Kızıltepe	X		28		X		247	-0	0,7
C5	Kızıltepe	X		28		X		400	-2	2,7
C5	Kızıltepe	X		28		X		216	-0	0,7
C5	Kızıltepe	X		28			X	185	-0	0,5
C5	Kızıltepe	X		28			X	165	-0	0,2
C11	Kızıltepe	X		110		X		276	-1	1,2
C11	Kızıltepe	X		110		X		243	-1	1,1
C11	Kızıltepe	X		110		X		257	-1	1,1
C11	Kızıltepe	X		110		X		228	-1	1,1
C11	Kızıltepe	X		110		X		212	-1	0,9
C11	Kızıltepe	X		110		X		217	-0	0,5
C11	Kızıltepe	X		110		X		236	-0	0,5
C11	Kızıltepe	X		110		X		255	-0	0,7
C11	Kızıltepe	X		110		X		248	-1	1,7
C11	Kızıltepe	X		110		X		227	-1	1,9
C11	Kızıltepe	X		110		X		242	-0	0,7
C11	Kızıltepe	X		110		X		265	-1	1,6
C11	Kızıltepe	X		110		X		220	-1	1,2
C11	Kızıltepe	X		110		X		222	-4	7
C11	Kızıltepe	X		110		X		246	-0	0,4
C28	Kızıltepe	X		40		X		300	-1	1,2
C28	Kızıltepe	X		40		X		270	-0	0,7
C28	Kızıltepe	X		40		X		275	-0	0,7
SA8	Kızıltepe		X		344		X	200	-1	1,6
SA8	Kızıltepe		X		344	X		277	-1	1,4
SA8	Kızıltepe		X		344	X		204	-1	0,9
SA8	Kızıltepe		X		344	X		246	-0	0,5
SA8	Kızıltepe		X		344	X		204	-0	0,4
SA8	Kızıltepe		X		344	X		214	-0	0,5
SA8	Kızıltepe		X		344	X		235	-1	1,2
SA8	Kızıltepe		X		344	X		200	-0	0,4
SA11	Kızıltepe		X		365	X		178	-1	1,2
SA11	Kızıltepe		X		365	X		176	-1	1,1
SA11	Kızıltepe		X		365	X		177	-1	1,2
SA11	Kızıltepe		X		365	X		178	-1	1,2

SA11	Kızıltepe		X		365	X		223	-1	1,9
SA11	Kızıltepe		X		365	X		157	-1	2,1
SA11	Kızıltepe		X		365	X		178	-1	1,2
SA11	Kızıltepe		X		365	X		213	-1	1,2
SA11	Kızıltepe		X		365	X		200	-1	1,1
SA11	Kızıltepe		X		365	X		180	-0	0,7
SA11	Kızıltepe		X		365	X		186	-1	1,2
SA11	Kızıltepe		X		365	X		182	-1	1,1
SA11	Kızıltepe		X		365	X		244	-0	0,7
SA11	Kızıltepe		X		365	X		259	-1	1,7
SA11	Kızıltepe		X		365	X		250	-1	1,6
SA11	Kızıltepe		X		365	X		180	-0	0,5
SA11	Kızıltepe		X		365	X		174	-0	0,7
SA11	Kızıltepe		X		365	X		246	-1	1,2
KEP2	Kepez		X		910	X		190	-2	3,2
KEP2	Kepez		X		910	X		187	-3	4,8
KEP2	Kepez		X		910	X		283	-0	0,7
KEP2	Kepez		X		910	X		212	-1	0,9
KEP2	Kepez		X		910	X		262	-1	0,9
KEP2	Kepez		X		910	X		210	-1	2,1
KEP2	Kepez		X		910	X		245	-1	1,1
KEP2	Kepez		X		910	X		227	-1	1,4
KEP2	Kepez		X		910	X		220	-0	0,4
KEP2	Kepez		X		910	X		214	-0	0,7
KEP2	Kepez		X		910	X		170	-0	0,5
KEP2	Kepez		X		910	X		210	-1	1,2
KEP2	Kepez		X		910	X		246	-1	1,1
KEP2	Kepez		X		910	X		205	-1	1,7
KEP2	Kepez		X		910	X		204	-1	1,7
KEP2	Kepez		X		910	X		207	-1	1,4
KEP2	Kepez		X		910	X		189	-0	0,5
SKAR1	Karadüz		X		1273	X		207	-0	0,5
SKAR1	Karadüz		X		1273	X		220	-0	0,5
SKAR1	Karadüz		X		1273	X		244	-0	0,5
SKAR1	Karadüz		X		1273	X		300	-0	0,7
SKAR1	Karadüz		X		1273	X		275	-1	0,9
SKAR1	Karadüz		X		1273	X		232	-0	0,5
SKAR1	Karadüz		X		1273	X		245	-1	2,1
SKAR1	Karadüz		X		1273	X		265	-1	1,2
SKAR1	Karadüz		X		1273	X		252	-1	1,4
SKAR1	Karadüz		X		1273	X		255	-0	0,5

SKAR1	Karadüz		X		1273	X		256	-0	0,5
SKAR1	Karadüz		X		1273	X		258	-1	2,1
SKAR1	Karadüz		X		1273	X		265	-1	1,9
SKAR1	Karadüz		X		1273	X		258	-1	1,4
SKAR1	Karadüz		X		1273	X		250	-1	1,4
SKAV3	Kavaklıdüz		X		1212	X		247	-1	2,4
SKAV3	Kavaklıdüz		X		1212	X		250	-1	2,2
SKAV3	Kavaklıdüz		X		1212	X		205	-1	1,6
SKAV3	Kavaklıdüz		X		1212	X		250	-1	1,7
SKAV3	Kavaklıdüz		X		1212		X	221	-1	2,4
SKAV3	Kavaklıdüz		X		1212		X	223	-1	2,4
SKAV3	Kavaklıdüz		X		1212	X		229	-2	2,9
SKAV3	Kavaklıdüz		X		1212	X		229	-2	2,6
SKAV3	Kavaklıdüz		X		1212	X		232	-1	1,4
SKAV3	Kavaklıdüz		X		1212	X		228	-1	1,2
SKAV3	Kavaklıdüz		X		1212	X		230	-1	1,4
SKAV3	Kavaklıdüz		X		1212		X	235	-2	3,6
SKAV3	Kavaklıdüz		X		1212		X	229	-14	17,8
SKAV3	Kavaklıdüz		X		1212		X	235	-14	17,6
SKAV3	Kavaklıdüz		X		1212	X		221	-2	3,7
SKAV3	Kavaklıdüz		X		1212	X		226	-0	0,4
SKAV3	Kavaklıdüz		X		1212	X		256	-0	0,7
SKAV3	Kavaklıdüz		X		1212	X		236	-0	0,7
SKAV3	Kavaklıdüz		X		1212	X		232	-1	1,4
SKAV3	Kavaklıdüz		X		1212	X		235	-1	2,4
SKAV3	Kavaklıdüz		X		1212	X		222	-0	0,4
SKAV1	Kavaklıdüz		X		1258	X		288	-2	3,2
SKAV1	Kavaklıdüz		X		1258	X		285	-1	1,9
SKAV1	Kavaklıdüz		X		1258	X		283	-2	3,2
SKAV1	Kavaklıdüz		X		1258	X		295	-1	1,7
SKAV1	Kavaklıdüz		X		1258	X		225	-0	0,2
SKAV1	Kavaklıdüz		X		1258	X		270	-0	0,4
SKAV1	Kavaklıdüz		X		1258	X		207	-0	0,5
SKAV1	Kavaklıdüz		X		1258	X		270	-1	0,9
SKAV1	Kavaklıdüz		X		1258	X		250	-2	3,1
SKAV1	Kavaklıdüz		X		1258	X		240	-3	4,2
SKAV1	Kavaklıdüz		X		1258	X		291	-2	2,6
SKAV1	Kavaklıdüz		X		1258	X		285	-1	2,4
SKAV1	Kavaklıdüz		X		1258	X		286	-1	2,4
SKAV1	Kavaklıdüz		X		1258	X		286	-1	2,4
SKAV1	Kavaklıdüz		X		1258	X		286	-1	2,4
SKAV1	Kavaklıdüz		X		1258	X		230	-1	2,1

SKAV1	Kavaklıdüz		X		1258	X		235	-1	2,1
SKAV1	Kavaklıdüz		X		1258	X		250	-0	0,5
SKAV1	Kavaklıdüz		X		1258	X		295	-0	0,5
SKAV1	Kavaklıdüz		X		1258	X		287	-0	0,5
SKAV1	Kavaklıdüz		X		1258	X		250	-0	0,5
SKAV1	Kavaklıdüz		X		1258	X		239	-0	0,4
SKAV1	Kavaklıdüz		X		1258	X		212	-1	1,9
SKAV1	Kavaklıdüz		X		1258	X		268	-2	3,4
SKAV1	Kavaklıdüz		X		1258	X		265	-2	2,7
SKAV1	Kavaklıdüz		X		1258	X		269	-1	2,2
SKAV1	Kavaklıdüz		X		1258	X		297	-1	1,9
SKAV1	Kavaklıdüz		X		1258	X		309	-1	1,9
SKAV1	Kavaklıdüz		X		1258	X		281	-1	1,9
SKAV1	Kavaklıdüz		X		1258	X		280	-1	1,7
SKAV1	Kavaklıdüz		X		1258	X		250	-3	4,7
SKAV1	Kavaklıdüz		X		1258	X		238	-3	4,2
SKAV1	Kavaklıdüz		X		1258	X		312	-3	4,3
SKAV1	Kavaklıdüz		X		1258	X		277	-3	4,7
SKAV1	Kavaklıdüz		X		1258		X	195	-1	1,9

Accordingly results, Kızıltepe have average fluid inclusion homogenization temperatures around 206°C, Kavaklıdüz and Karadüz both contain significantly higher average homogenization temperatures 252°C, Kepez have 216°C (Table 2.6). As for % NaCl results, four areas at issue (Kiziltepe, Kepez, Karadüz and Kavaklidüz) have salinity between %1 and %2. All of the results show the epithermal system.

Table 2.6 Descriptive statistics of fluid inclusion data for each Sindirgi Prospects.

Descriptive Statistics

Variable	*Area*	*Min %NaCl*	*Max %NaCl*	*N*	*Mean*	*Median*	*StDev*
%NaCl	Core (drill)	0,2	7	64	1,4	1,1	1,1
	Kızıltepe	0,4	2,1	26	1,1	1,2	0,46
	Kavaklıdüz	0,2	17,8	56	2,61	2,1	3,16
	Karadüz	0,5	2,1	15	1,07	0,9	0,61
	Kepez	0,4	4,8	17	1,43	1,1	1,11

Variable	*Area*	*Min Th*	*Max Th*	*N*	*Mean*	*Median*	*StDev*
Th°C	Core (drill)	160	402	64	260,3	244,5	65,42
	Kızıltepe	157	277	26	206,19	200	32,02
	Kavaklıdüz	195	312	56	252,8	250	29,2
	Karadüz	207	300	15	252,13	255	22,09
	Kepez	170	283	17	216,53	210	28,81

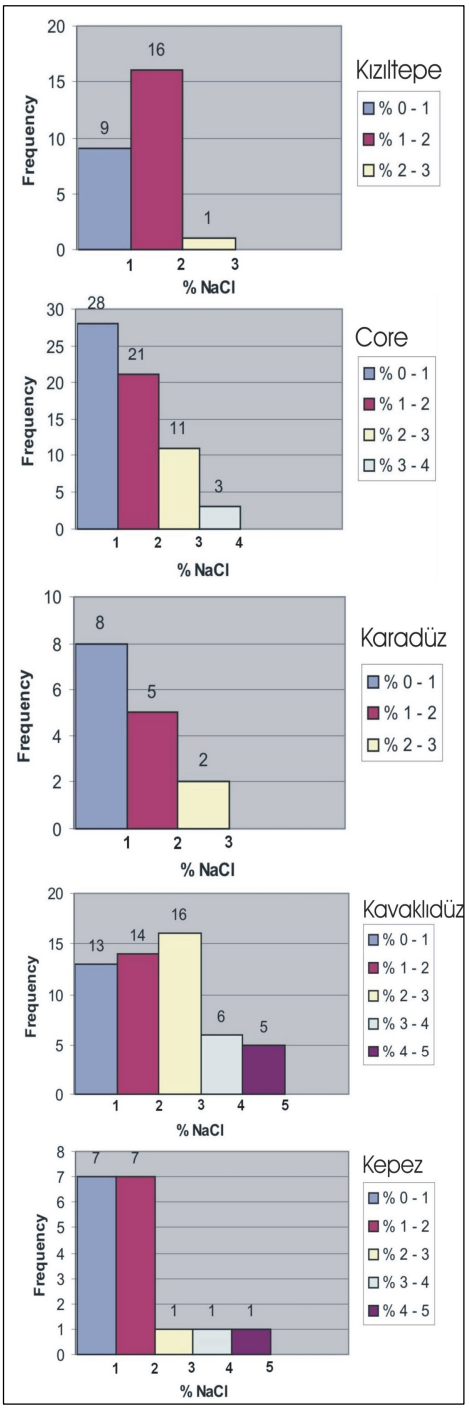

Figure 2.19 Summary of fluid inclusion % NaCl data for Sindirgi Prospects (Kızıltepe, core samples were taken from Kızıltepe, Karadüz, Kavaklıdüz and Kepez).

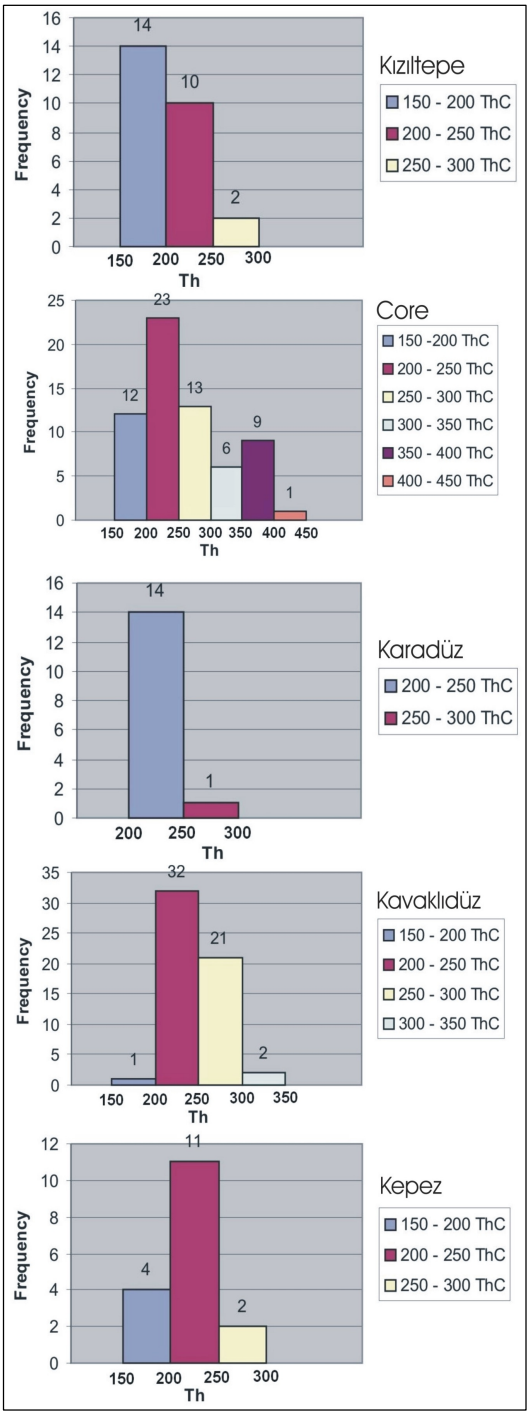

Figure 2.20 Summary of fluid inclusion Th°C data for Sindirgi Prospects (Kızıltepe, core samples were taken from Kızıltepe, Karadüz, Kavaklıdüz and Kepez).

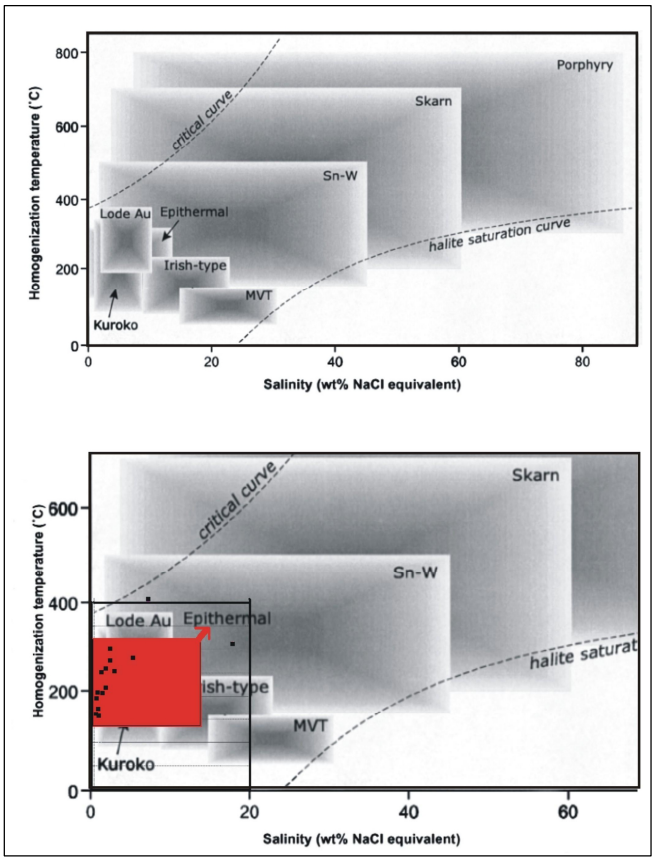

Figure 2.21 Summary homogenization temperature–salinity diagram illustrating typical ranges for fluid inclusions from different deposit types.

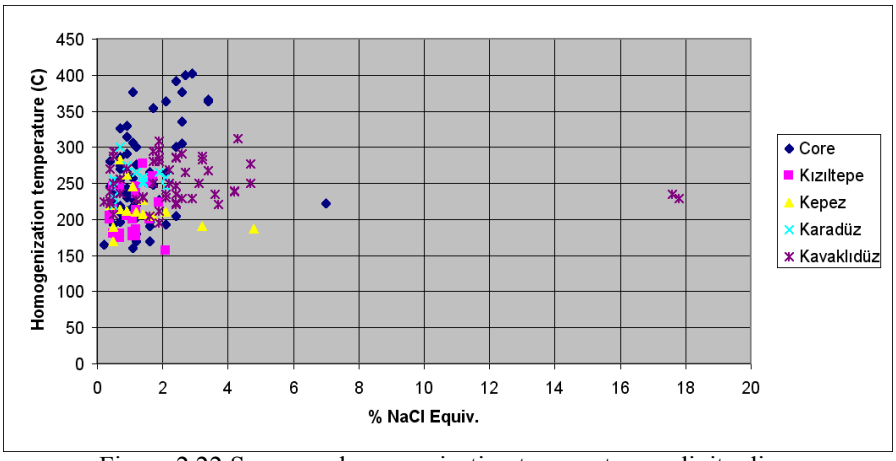

Figure 2.22 Summary homogenization temperature–salinity diagram

Table 2.7 Descriptive fluid inclusion statistics (Th and % NaCl) for each Prospect at Sindirgi..

Core Sample

Variable	*Sample No*	*Min Th*	*Max Th*	*N*	*Mean*	*Median*	*StDev*
Th	C1	169	402	33	275,09	264	76,62
	C5	160	400	13	241,69	218	68,81
	C11	212	276	15	239,6	242	18,73
	C22	x	x	x	x	x	x
	C28	270	300	3	281,67	275	16,07
Variable	*Sample No*	*Min %NaCl*	*Max %NaCl*	*N*	*Mean*	*Median*	*StDev*
%NaCl	C1	0,5	3,4	33	1,6	1,2	0,9
	C5	0,2	2,7	13	1	0,7	0,78
	C11	0,4	7	15	1,44	1,1	1,6
	C22	x	x	x	x	x	x
	C28	0,7	1,2	3	0,87	0,7	0,29

Kızıltepe

Variable	*Sample No*	*Min Th*	*Max Th*	*N*	*Mean*	*Median*	*StDev*
Th	SA5	x	x	x	x	x	x
	SA8	157	180	8	174,75	177,5	7,4
	SA11	180	277	18	220,17	213,5	28,52
Variable	*Sample No*	*Min %NaCl*	*Max %NaCl*	*N*	*Mean*	*Median*	*StDev*
%NaCl	SA5	x	x	x	x	x	x
	SA8	0,4	1,6	8	0,86	0,7	0,48
	SA11	0,5	2,1	18	1,2	1,2	0,42

Karadüz

Variable	*Sample No*	*Min Th*	*Max Th*	*N*	*Mean*	*Median*	*StDev*
Th	SKar1	207	300	15	252,13	255	22,09
Variable	*Sample No*	*Min %NaCl*	*Max %NaCl*	*N*	*Mean*	*Median*	*StDev*
%NaCl	SKar1	0,5	2,1	15	1,07	0,9	0,61

Kepez

Variable	*Sample No*	*Min Th*	*Max Th*	*N*	*Mean*	*Median*	*StDev*
Th	Kep2	170	283	17	216,53	210	28,81
Variable	*Sample No*	*Min %NaCl*	*Max %NaCl*	*N*	*Mean*	*Median*	*StDev*
%NaCl	Kep2	0,4	4,8	17	1,43	1,1	1,11

Kavaklıdüz

Variable	*Sample No*	*Min Th*	*Max Th*	*N*	*Mean*	*Median*	*StDev*
Th	SKav3	205	256	21	231,95	230	11,68
	SKav1	195	312	35	265,31	270	29,47
Variable	*Sample No*	*Min %NaCl*	*Max %NaCl*	*N*	*Mean*	*Median*	*StDev*
%NaCl	SKav3	0,4	17,8	21	3,38	2,2	4,85
	SKav1	0,2	4,7	35	2,16	2,1	1,3

2.6 $^{40}Ar/^{39}Ar$ results

Adularia from quartz-adularia veins was selected for $^{40}Ar/^{39}Ar$ geochronology in order to establish the temporal relationship between magmatism, deformation and mineralization at Kiziltepe. The sample was handpicked under binocular microscope to an estimated purity of >99 %, and then cleaned in an ultrasonic bath with deionized water and acetone. 200 mg samples were irradiated at McMaster Nuclear Reactor at McMaster University, Ontario, Canada. For $^{40}Ar/^{39}Ar$ analysis, a plateau segment consists of 3 or more contiguous gas fractions having analytically indistinguishable ages (i.e., all plateau steps overlap in age at $\pm 2\sigma$ analytical error) and comprising a significant portion of the total gas released (typically >50%). Total gas (integrated) ages are calculated by weighting by the amount of ^{39}Ar released, whereas plateau ages are weighted by the inverse of the variance. For each sample inverse isochronal diagrams are examined to check for the effects of excess argon. Reliable isochrones are based on the MSWD criteria of Wendt and Carl (1991) and, as for plateaus, must comprise contiguous steps and a significant fraction of the total gas released. All analytical data are reported at the 1σ confidence level.

The samples that choose from the study area were run as conventional furnace step heating analyses. This type of sample run produces what is referred to as an apparent age spectrum. The "apparent" derives from the fact that ages on an age spectrum plot are calculated assuming that the non-radiogenic argon (often referred to as trapped, or initial argon) is atmospheric in isotopic composition ($^{40}Ar/^{36}Ar$ = 295.5). If there is excess argon in the sample ($^{40}Ar/^{36}Ar > 295.5$) then these ages will be older than the actual age of the sample. Samples analyzed by the $^{40}Ar/^{39}Ar$ method at the University of Nevada Las Vegas were wrapped in Al foil and stacked in 6 mm inside diameter sealed fused silica tubes. Individual packets averaged 3 mm thick and neutron fluence monitors (FC-2, Fish Canyon Tuff sanidine) were placed every 5-10 mm along the tube.

Four samples were sent for analysis (Figure 2.23) and three of them returned the reliable age results (Figure 2.25).

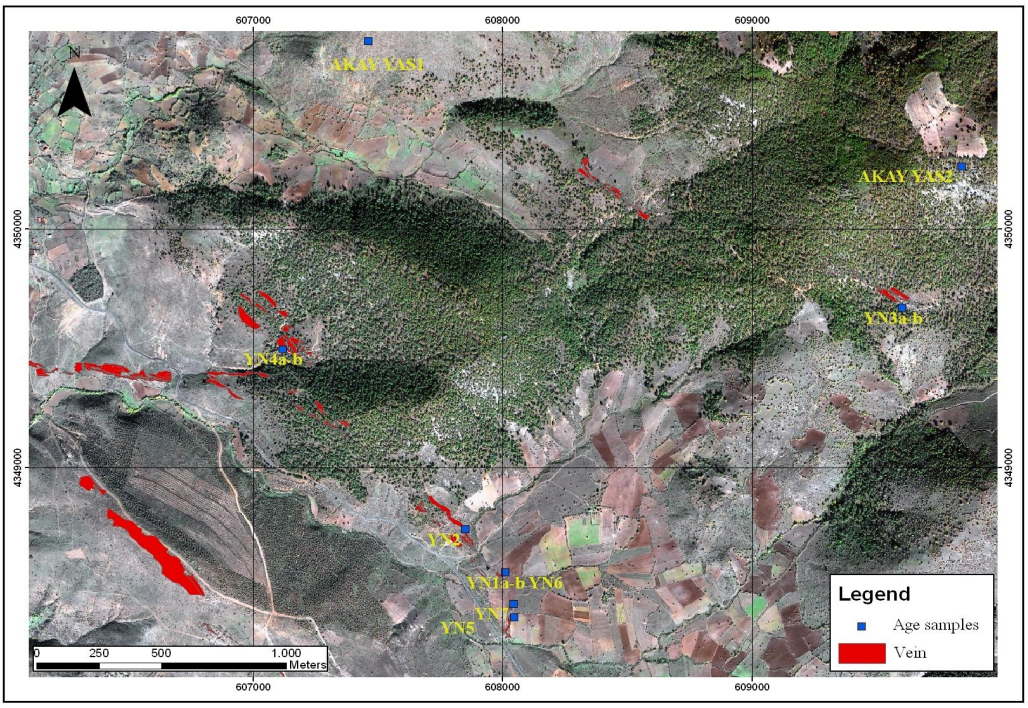

Figure 2.23 Sample locations for age determinations.

Sample YN5 (adularia) has generally the concordant age spectrum, with most ages ~18.3 Ma. Steps 3-6 (65% of the ^{39}Ar released) define a slightly older, but analytically indistinguishable, plateau age of 18.27 ± 0.11 Ma (Figure 2.24). However, the $^{40}Ar/^{36}Ar$ intercept is anomalously low, making this isochron age suspect. The plateau age should be considered the most reliable for this sample. The age for this sample should be considered to be quite reliable, as it is generally a well behaved, and a fairly ideal sample.

Sample AkayYas 2 (817) (dacite) shows some slight discordance in the first few steps, this sample produced an ideal, flat age spectrum. Steps 8-11 (78% of the ^{39}Ar released) define an analytically indistinguishable plateau age of 18.96 ± 0.11 Ma (Figure 2.24). This sample should be considered highly reliable.

Sample AkayYas 1 (756) (dacite) is similar to 817 dacite described above. The age spectrum is nearly ideal and perfectly flat, with only some minor discordance. Steps 5-11 (52% of the ^{39}Ar released) define an indistinguishable plateau age of 19.82 ± 0.14 Ma (Figure 2.24). This sample should be considered highly reliable.

Sample YN4A (Adularia and Quartz) has the very discordant age spectrum. This sample should not be considered reliable.

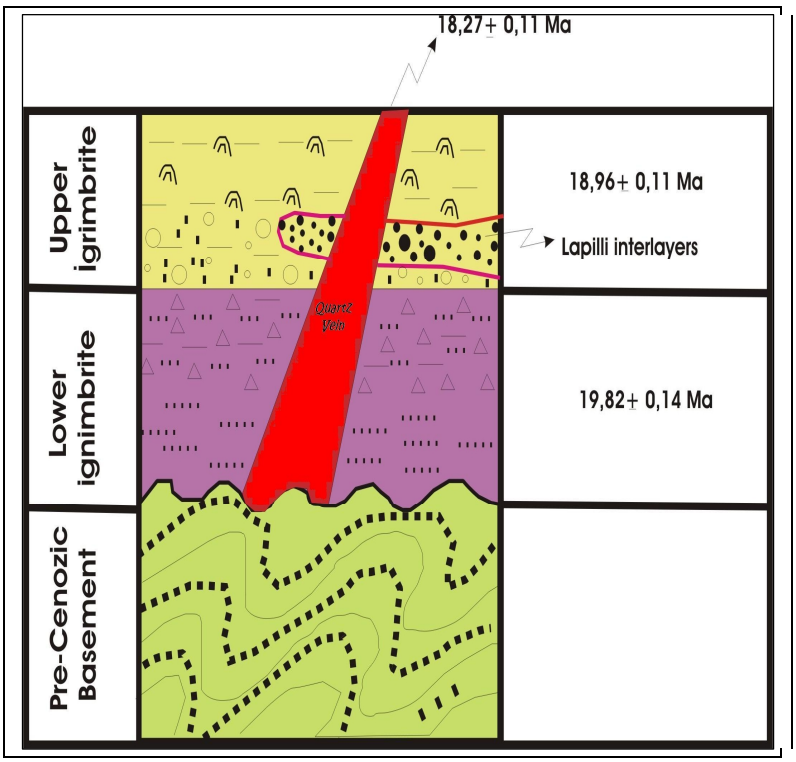

Figure 2.24 The age relationship between ignimbrites and Kiziltepe Au-Ag-Bearing quartz vein mineralization.

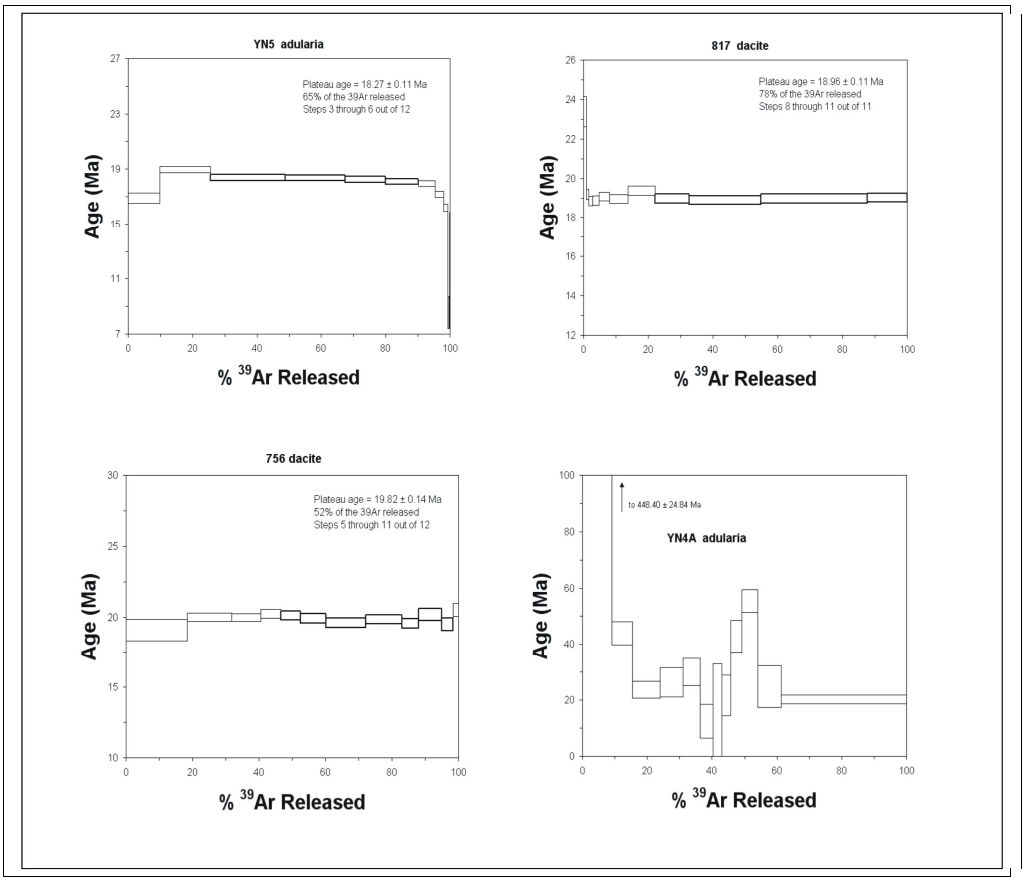

Figure 2.25 Step-heating spectra of adularia and biotite from Sindirgi.

All of age ^{40} Ar/^{39} Ar results suggested that the age of lower ignimbrite as 19.82 ± 0.14 Ma, upper ignimbrite as 18.96 ± 0.11 Ma and quartz vein mineralization as 8.27 ± 0.11 Ma.

2.6 $^{40}Ar/^{39}Ar$ results

Adularia from quartz-adularia veins was selected for $^{40}Ar/^{39}Ar$ geochronology in order to establish the temporal relationship between magmatism, deformation and mineralization at Kiziltepe. The sample was handpicked under binocular microscope to an estimated purity of >99 %, and then cleaned in an ultrasonic bath with deionized water and acetone. 200 mg samples were irradiated at McMaster Nuclear Reactor at McMaster University, Ontario, Canada. For $^{40}Ar/^{39}Ar$ analysis, a plateau segment consists of 3 or more contiguous gas fractions having analytically indistinguishable ages (i.e., all plateau steps overlap in age at $\pm 2\sigma$ analytical error) and comprising a significant portion of the total gas released (typically >50%). Total gas (integrated) ages are calculated by weighting by the amount of ^{39}Ar released, whereas plateau ages are weighted by the inverse of the variance. For each sample inverse isochronal diagrams are examined to check for the effects of excess argon. Reliable isochrones are based on the MSWD criteria of Wendt and Carl (1991) and, as for plateaus, must comprise contiguous steps and a significant fraction of the total gas released. All analytical data are reported at the 1σ confidence level.

The samples that choose from the study area were run as conventional furnace step heating analyses. This type of sample run produces what is referred to as an apparent age spectrum. The "apparent" derives from the fact that ages on an age spectrum plot are calculated assuming that the non-radiogenic argon (often referred to as trapped, or initial argon) is atmospheric in isotopic composition ($^{40}Ar/^{36}Ar$ = 295.5). If there is excess argon in the sample ($^{40}Ar/^{36}Ar > 295.5$) then these ages will be older than the actual age of the sample. Samples analyzed by the $^{40}Ar/^{39}Ar$ method at the University of Nevada Las Vegas were wrapped in Al foil and stacked in 6 mm inside diameter sealed fused silica tubes. Individual packets averaged 3 mm thick and neutron fluence monitors (FC-2, Fish Canyon Tuff sanidine) were placed every 5-10 mm along the tube.

Four samples were sent for analysis (Figure 2.23) and three of them returned the reliable age results (Figure 2.25).

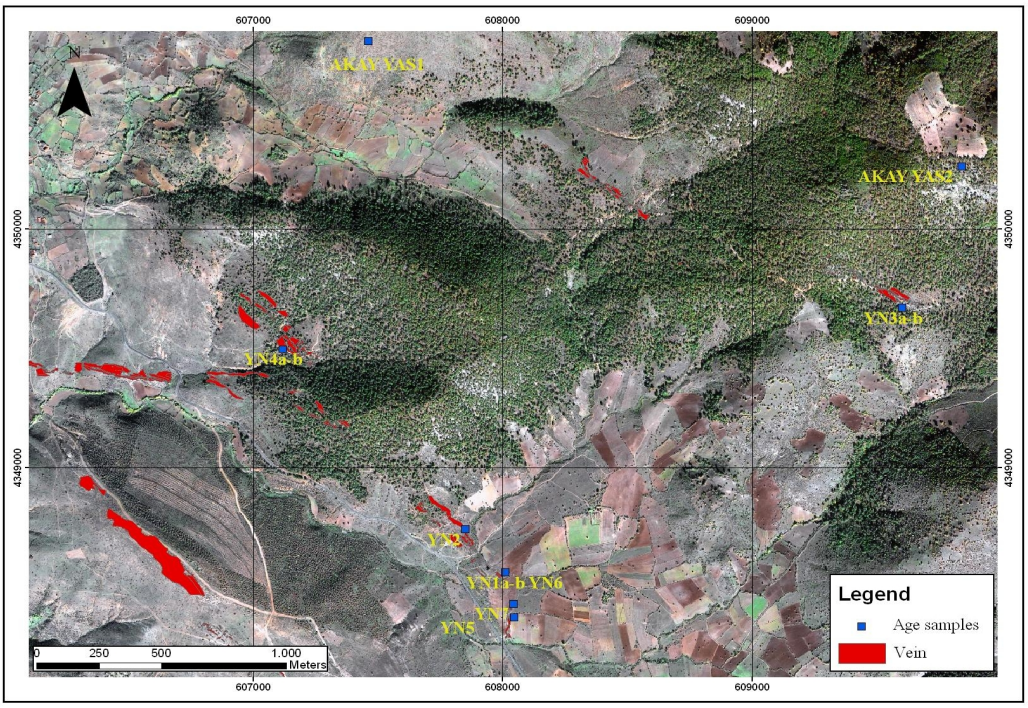

Figure 2.23 Sample locations for age determinations.

Sample YN5 (adularia) has generally the concordant age spectrum, with most ages ~18.3 Ma. Steps 3-6 (65% of the ^{39}Ar released) define a slightly older, but analytically indistinguishable, plateau age of 18.27 ± 0.11 Ma (Figure 2.24). However, the $^{40}Ar/^{36}Ar$ intercept is anomalously low, making this isochron age suspect. The plateau age should be considered the most reliable for this sample. The age for this sample should be considered to be quite reliable, as it is generally a well behaved, and a fairly ideal sample.

Sample AkayYas 2 (817) (dacite) shows some slight discordance in the first few steps, this sample produced an ideal, flat age spectrum. Steps 8-11 (78% of the ^{39}Ar released) define an analytically indistinguishable plateau age of 18.96 ± 0.11 Ma (Figure 2.24). This sample should be considered highly reliable.

Sample AkayYas 1 (756) (dacite) is similar to 817 dacite described above. The age spectrum is nearly ideal and perfectly flat, with only some minor discordance. Steps 5-11 (52% of the ^{39}Ar released) define an indistinguishable plateau age of 19.82 ± 0.14 Ma (Figure 2.24). This sample should be considered highly reliable.

Sample YN4A (Adularia and Quartz) has the very discordant age spectrum. This sample should not be considered reliable.

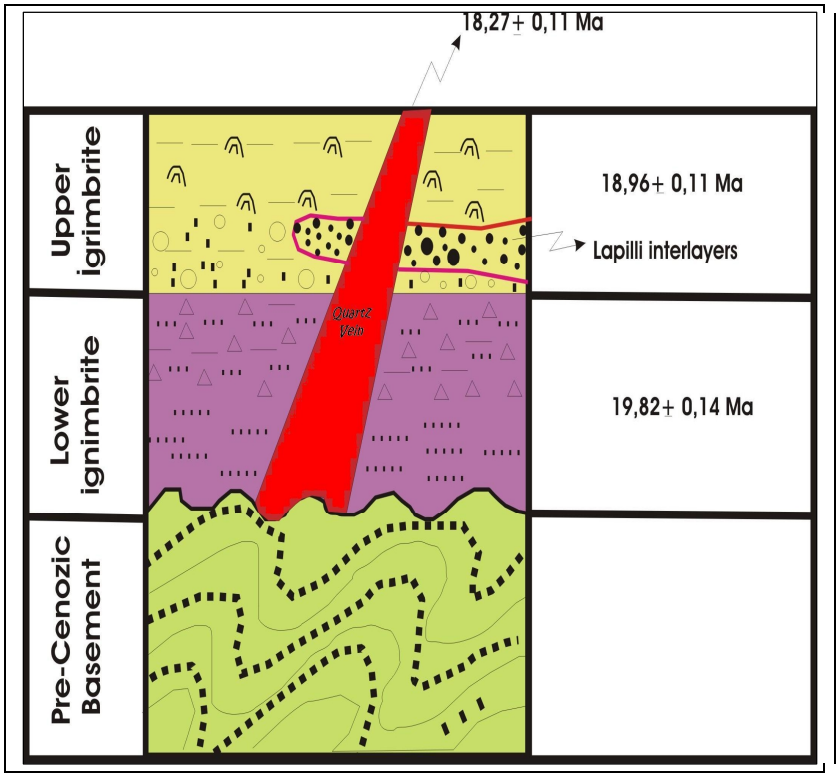

Figure 2.24 The age relationship between ignimbrites and Kiziltepe Au-Ag-Bearing quartz vein mineralization.

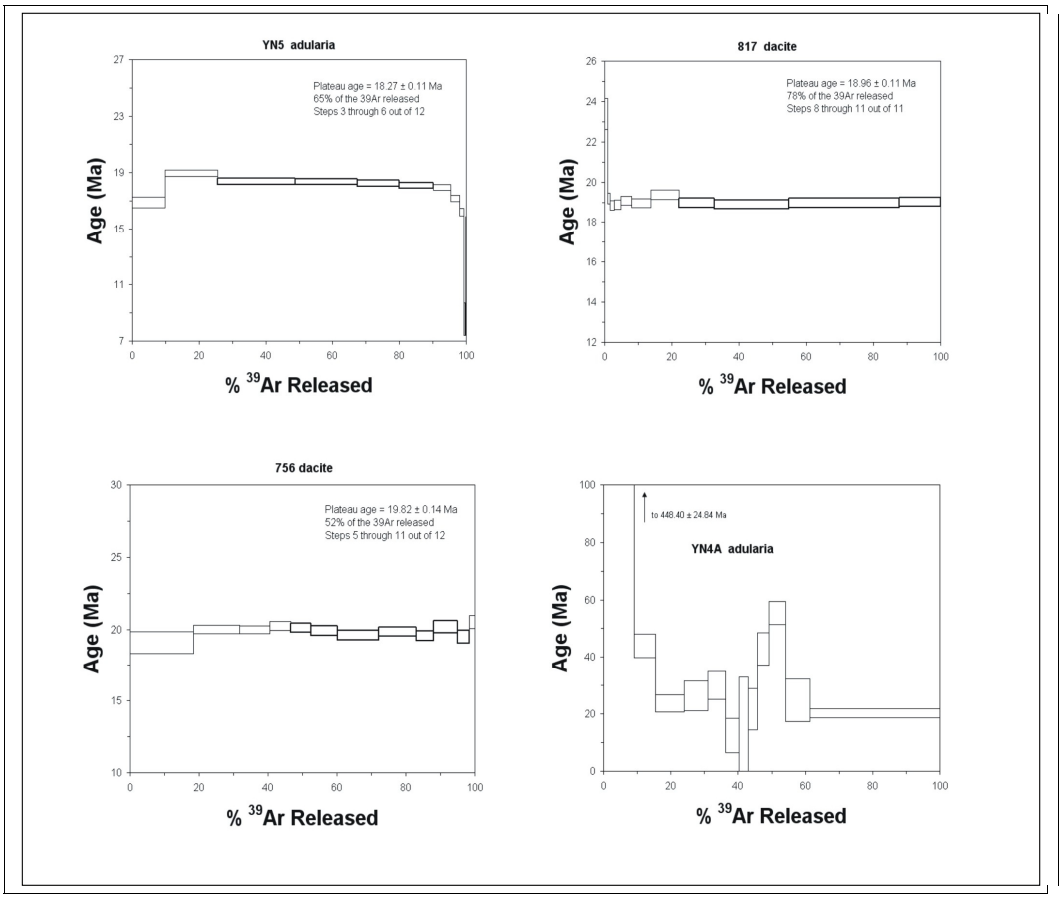

Figure 2.25 Step-heating spectra of adularia and biotite from Sindirgi.

All of age $^{40}Ar/^{39}Ar$ results suggested that the age of lower ignimbrite as 19.82 ± 0.14 Ma, upper ignimbrite as 18.96 ± 0.11 Ma and quartz vein mineralization as 8.27 ± 0.11 Ma.

CHAPTER THREE
SUMMARY and CONCLUSIONS

Hydrothermal systems have been defined (Berger and Eimon 1983) as epithermal systems if they formed within 1 km of the surface, at temperature less than 300°C (mainly 150°-250°C) and from a fluid of meteoric origin, possibly with some magmatic input (White and Hedenquist. 1990). Epithermal systems are also distinguished from other deposit types by gold to silver ratios (Hedenquist and Reid. 1987; Morrison et al.. 1991) host rock composition (Bonham. 1986) and geological settings (White and Hedenquist. 1990). Many workers differentiate two styles of epithermal gold deposits which are initially distinguished as adularia-sericite and acid-sulfate (Hayba et al.. 1985; Heald et al.. 1987) and more recently as low and high sulfidation systems. The sediment hosted replacement gold deposits are no longer recognized as necessarily epithermal. Leach and Corbett (1995) epithermal systems are defined on the basis of their crustral levels (I.e porphyry, mesothermal, epithermal) and fluid chemistry (low or high sulfidation).

The study area is an example for low sulfidation gold deposit evidenced by the recognition of chalcedonic quartz, adularia, illite/sericite and mixed-layered smectite minerals along with moderately dominant colloform/crustiform banding textures. Massive chalcedonic texture forms under conditions of intermediate silica supersaturation with respect to quartz. Low temperature (below about 180°C), during and after deposition is responsible for the low crystallinity maintained in this textures.

The wall rock alteration assemblages, along with quartz, adularia and calcite include K-mica, chlorite and pyrite. Interstratified illite-smectite and smectite clays plus kaolinite can occur on the margins of the system, where temperatures were cooler and vapor condensates may have been present. Thus, alteration mineralogy shows the characteristics low sulfidation systems. Adularia within geothermal fields

is an indicator high permeability and indirectly forms as a by-product of boiling (Simmons and Browne, 2000). Interpretation of clay clay fractions identified kaolinite, illite, smectite and interstratified illite-smectite.

Propylitic alteration consisting mainly of pyrite and chlotite along with minor illite and smectite encompasses in the outer zones of argillic alteration. The argillic zone proximal to major quartz veins is dominated by quartz ((quartz is the gangue phase in adularia sericite gold-silver systems (Hayba et al., 1985)) + K-Feldspar (adularia) + illite/smectite± kaolinite (nacrite).

Negative correlation coefficients between SiO_2 and REE (Table 2.4) and positive correlations coefficients between K and REE are very strong. Although there appears to be very strong correlation coefficients among Ba, Rb,Sr and REE, no correlations are appear between SiO_2 and Au, Ag, Sb.

Correlation coefficients between Au and Ag is very strong (R=0,96). It is important to consider that Ag/Au ratio ranges from10 to 22. This ratio is important as an exploration guide in establishing the nature of the system as well as elucidating metal enrichment and zoning (Cole and Drummond, 1986). If epithermal systems with Ag/Au ratios (as is the case of study area) are ~1, they contain mainly electrum and free gold. Au -thisulfide complex is dominant and the temperature of formation is less than 250°C.

Kızıltepe have average fluid inclusion homogenization temperatures around 206°C, Kavaklidüz and Karadüz both contain significantly higher average homogenization temperatures up to 252°C, Kepez have 216°C. As for % NaCl results, four areas including Kiziltepe, Kepez, Karadüz and Kavaklidüz have salinity values between %1 and %2. All these results point to a low sulfidation adularia-sericite-type epithermal system.

All of age $^{40}Ar/^{39}Ar$ results suggested that the age of lower ignimbrite as 19.82 ± 0.14 Ma, upper ignimbrite as 18.96 ± 0.11 Ma and quartz vein mineralization as 8.27 ± 0.11 Ma, indicating that gold mineralization postdates both ignimbrite units.

Alteration mineralogy and fluid inclusion studies suggested that, The Sindirgi gold mineralization represents the medium levels of low sulfidation system. Remaining mineralization may represent the deeper levels of the low sulfidation system.

REFERENCES

Akay, E., 2007. Geology of Kiziltepe prospect and surroundings (SINDIRGI-BALIKESIR). *Unpublished reports.*

Altunkaynak, Ş., Yilmaz, Y., 1998. The mount Kozak magmatic complex, Western Anatolia. *Journal of Volcanology and Geothermal Research 85, 211-231.*

Bau, M., 1991. Rare earth element mobility during hydrothermal and metamorphic fluid-rock interaction and the significance of the oxidation stage of europium. *Chemical Geology 93, 219-230.*

Berger, B.R., and Eimon, P.I., 1983, Conceptual models of epithermal metal deposits in Shanks, W.C., ed., Cameron Volume on Unconventional Mineral Deposits: *Society of Mining Engineers, New York, p. 191-205.*

Bi, X., Hu, R., Cornell, D.H., 2004. The alkaline porphyry associated Yao'an gold deposit, Yunnan, China: *rare earth element and stable isotope evidence for magmatic-hydrothermal ore formation. Mineralium Deposita 39, 21–30.*

Bierlein, F.P., Waldron, H.M., Arne, D.C., 1999. Behaviour of rare earth and high field strength elements during hydrothermal alteration of meta-turbidites associated with mesothermal gold mineralization in central Victoria, Australia. *Journal of Geochemical Exploration 67, 109–125.*

Bonham, H. F., 1986. Models for volcanic-hosted epithermal precious metal deposits: A review, in proceedings of Symposium 5: volcanism, hydrothermal systems and related mineralization, February 1986, Auckland: *Auckland, International Volcanological Congress, p. 13-18.*

Browne, P.R.L., 1978. Hydrothermal alteration in active geothermal fields. *Annual Review of Earth and Planetary Science 6, 229–250.*

Cole, D.R., Drummond, S.E., 1986. The effect of transport and boiling on Ag/Au ratios in hydrothermal solutions: a preliminary assessment and possible implications of the formation of epithermal precious-metal ore deposits. *Journal of Geochemical Exploration 25, 45–79.*

Ercan, T., Satir, M., Steinitz, G., Dora, Ö., Sarifakioglu, E., Adis, C., Walter, H.J., Yıldırım, T., 1995. Biga yarimadasi ile Gokceada, Bozcaada ve Tavşan adalarindaki (KB Anadolu) Tersiyer volkanizmasinin ozellikleri. Maden Tetkik ve Arama Enstitusu Dergisi 117, 55-86 (in Turkish with English Abstract).

Ercan, T., Turkecan, A., Akyürek, B., Günay, E., Cevıkbaş, A., Ateş, M., Can, B., Erkan, M. Ozkısışçı, E., 1984. The geology of Dikili-Bergama-Çandarlı area (Western Anatolia) and petrology of the magmatic rocks. *Jeoloji Mühendisliği Dergisi 20, 47-60 (Turkish with an English abstract).*

Fournier, R.O., 1985. The behavior of silica in hydrothermal solutions. *Reviews in Economic Geology 2, 45–61.*

Heald, P., Foley, N.K., Hayba, D.O., 1987. Comparative anatomy of volcanic-hosted epithermal deposits: acid-sulfate and adularia–illite types. *Economic Geology 82, 1–26.*

Hedenquist, J.W., Browne, P.R.L., 1989. The evolution of the Waiotopu geother mal system, New Zealand, based on the chemical and isotopic composition of its fluids, mineral and rocks. *Geochimica et Cosmochimica Acta 53, 2235– 2257.*

Leach, T.M., Corbett, G.J., 1995. Characteristics of low sulfidation Au-Cu systems in the southwest pacific, in Pacific Rim Congress 95, 19-22 November 1995, Auckland, New Zeeland, proceedings, Carlton South. *The Australian Institute of Mining and Metallurgy, 327-332.*

Leach, T.M., Corbett, G.J., 2001. Characteristics of low sulfidation Au–Cu systems in the southwest Pacific. Pacific Rim Congress 95, 19–22 November 1995, Auckland, New Zealand, Proceedings. *The Australasian Institute of Mining and Metallurgy, pp. 327–332.*

Mckenzie, D. Yilmaz, Y., 1991. Deformation and volcanism in western Turkey and Aegean. *Bulletin of the Technical University of Istanbul 44,345-373.*

Michard, A., 1989. Rare earth element systematics in hydrothermal fluids. *Geo chimica et Cosmochimica Acta 53, 745-750.*

Morrison, G., Guoyi, D., Subhash, J., 1991. Textural zoning in epithermal quartz veins. James Cook University, Townsville, Australia, *unpublished AMIRA report, p. 247, 1-19.*

Palacios, C.M., Hein, U.F., Dulski, P., 1986. Behavior of rare earth elements during hydrothermal alteration at the Buena Esperanza copper–silver deposit, north Chile. *Earth and Planetary Science Letters 80, 208–216.*

Pirajno, F., 1995. Volcanic-hosted epithermal systems in northwest Turkey, *South. African Journal Geology, 98/1. 13/24.*

Şener, K., 2006. Galata Madencilik AŞ, Turkey. *Unpublished company reports.*

Seyitoğlu, G., and Scott, B., 1991, Late Cenozoic crustal extension and basin formation in west Turkey. *Geological Magazine 128, 155-166.*

Seyitoğlu, G., Anderson, D., Nowell, G., Scoot, B., 1997. The evolution from Miocene potassic to Quaternary sodic magmatism in Western Turkey: implications for enrichment processes in lithospheric mantle. *Journal of Volcanology and Geothermal Research 76, 127-147.*

Simmons. S. F..and Browne. P.R.L.. 2000. Hyrothermal minerals and precious metals in the Broadlands-Ohaaki Geothermal System: Implications for und erstanding low-sufidation epithermal environments: *Economic Geology v. 95.p.971-1000.*

Terakado, Y.,Fujitani, T, 1998. Behavior of the rare earth elements and other trace elements during interactions between acidic hydrothermal solutions and silicic volcanic rocks, southwestern Japan. *Geochimica et Cosmochimica Acta 62, 1903-1917.*

White, N.C., Hedenquist, J.W., 1990. Epithermal environments and styles of mineralization: variation and their causes, and guide lines for exploration. *Journal of Geochemical Exploration 36, 445–474.*

Wright, J., Piantone, H., cassard , D., Özaslan, G., 1996. Results of 1995 field program western Anatolia, *LaSource Project Generation Group-N2344, Orleans, France.*

Yilmaz, H., 2002, Ovacik gold deposit – An example of quartz-adularia-type gold mineralization in Turkey. *Economic Geology 97, 1829-1839.*

Yilmaz, H., 2007, Low-sulfidation type Au-Ag mineralization at Bergama, Izmır, Turkey.

Yilmaz, Y., 1989. The origin of young volcanic rocks of western Turkey. In: Sengor, A.C.M. (Ed), Tectonic Evolution of the Tethyan Region. *Kluver Academic Publishers, pp. 159-189.*

Zanchi, A., Kissel, C., Tipirdamaz, C., 1990. Continental deformation in western Turkey: a structural and paleomagnetic approach. *In abstract International Earth Science Congress on Aegean Regions, October 1–6, 1990. Dokuz Eylul University, İzmir, Turkey, pp. 357–367.*

Zanchi, A., Kissel, C., Tipirdamaz, C., 1993. Late Cenozoic and quaternary brittle continental deformation in western Turkey. *Bulletin Sociéte Geologique de France 164, 507–517.*

APPENDIX 1. XRD DIFFROCTOGRAM PROFILES

(From 2Q = 2° to 75°)

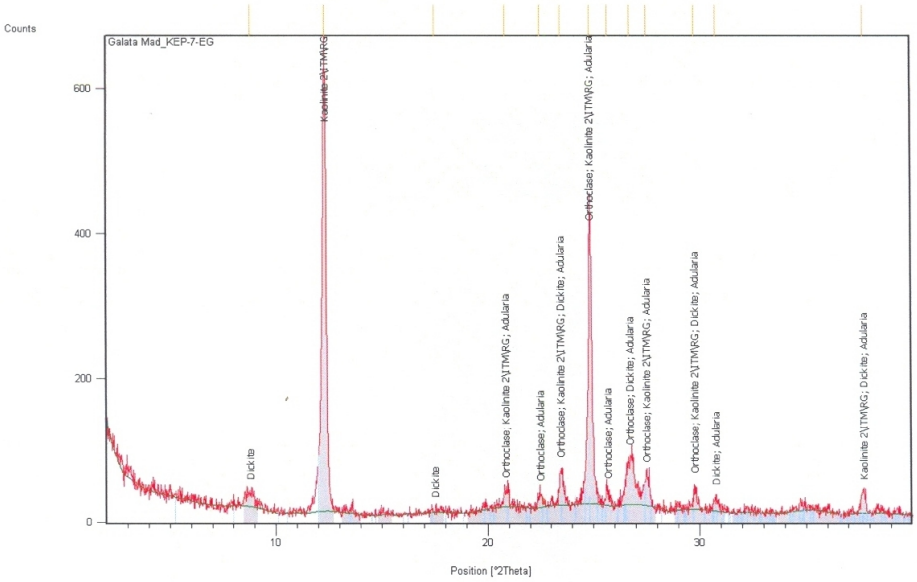
Counts
Galata Mad_KEP-7-EG
600
400
200
0
Dickite
Kaolinite 2\TMRG
Dickite
Orthoclase; Kaolinite 2\TMRG; Adularia
Orthoclase; Adularia
Orthoclase; Kaolinite 2\TMRG; Dickite; Adularia
Orthoclase; Adularia
Orthoclase; Dickite; Adularia
Orthoclase; Kaolinite 2\TMRG; Adularia
Orthoclase; Kaolinite 2\TMRG; Dickite; Adularia
Dickite; Adularia
Kaolinite 2\TMRG; Dickite; Adularia
10
20
30
Position [°2Theta]

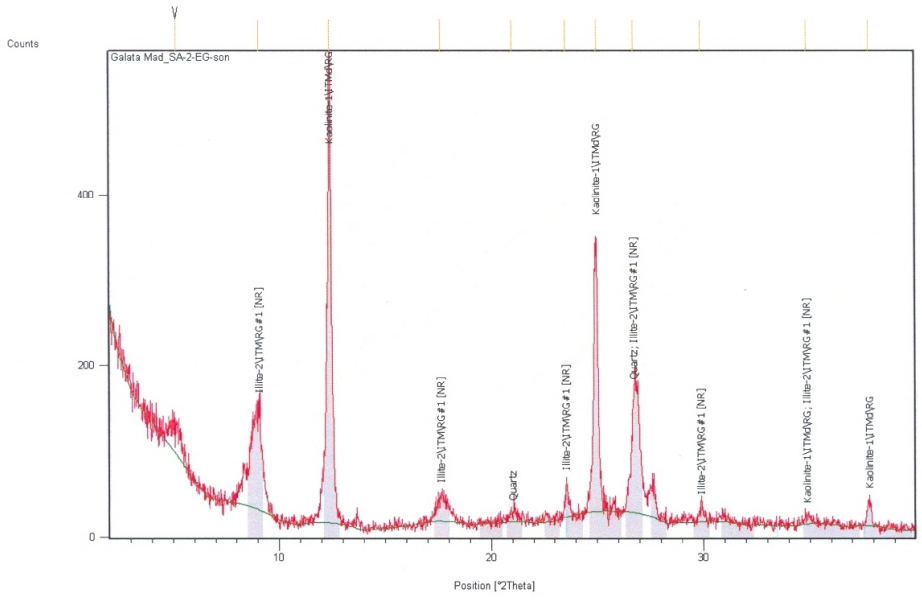
Counts
Galata Mad_SA-2-EG-son
400
200
0
Illite-2\TMRG#1 [NR]
Kaolinite-1\TMRG
Illite-2\TMRG#1 [NR]
Quartz
Illite-2\TMRG#1 [NR]
Kaolinite-1\TMRG
Quartz; Illite-2\TMRG#1 [NR]
Illite-2\TMRG#1 [NR]
Kaolinite-1\TMRG; Illite-2\TMRG#1 [NR]
Kaolinite-1\TMRG
10
20
30
Position [°2Theta]

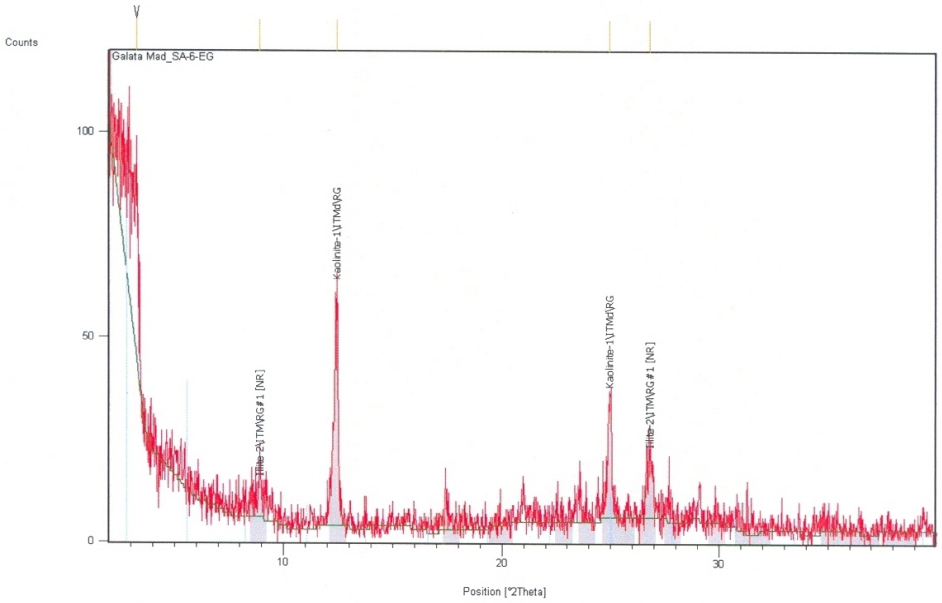
Counts
Galata Mad_SA-6-EG
100
50
0
Illite-2\TMR\#1 [NR]
Kaolinite-1\TMR\RG
Kaolinite-1\TMR\RG
Illite-2\TMR\#1 [NR]
10
20
30
Position [°2Theta]

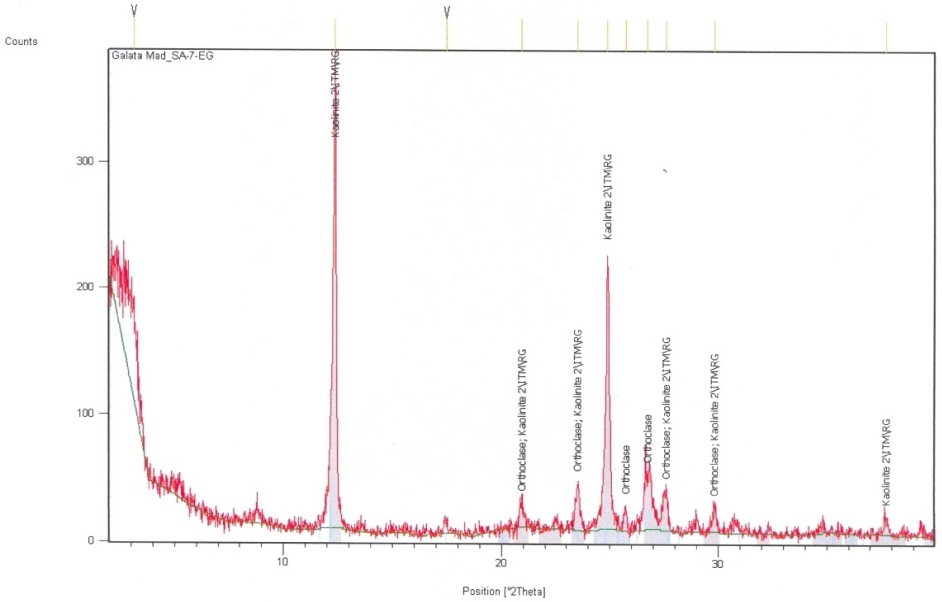
Counts
Galata Mad_SA-7-EG
300
200
100
0
Kaolinite-2\TMR\RG
Orthoclase; Kaolinite 2\TMR\RG
Orthoclase; Kaolinite 2\TMR\RG
Kaolinite 2\TMR\RG
Orthoclase
Orthoclase
Orthoclase; Kaolinite 2\TMR\RG
Orthoclase; Kaolinite 2\TMR\RG
Kaolinite 2\TMR\RG
10
20
30
Position [°2Theta]

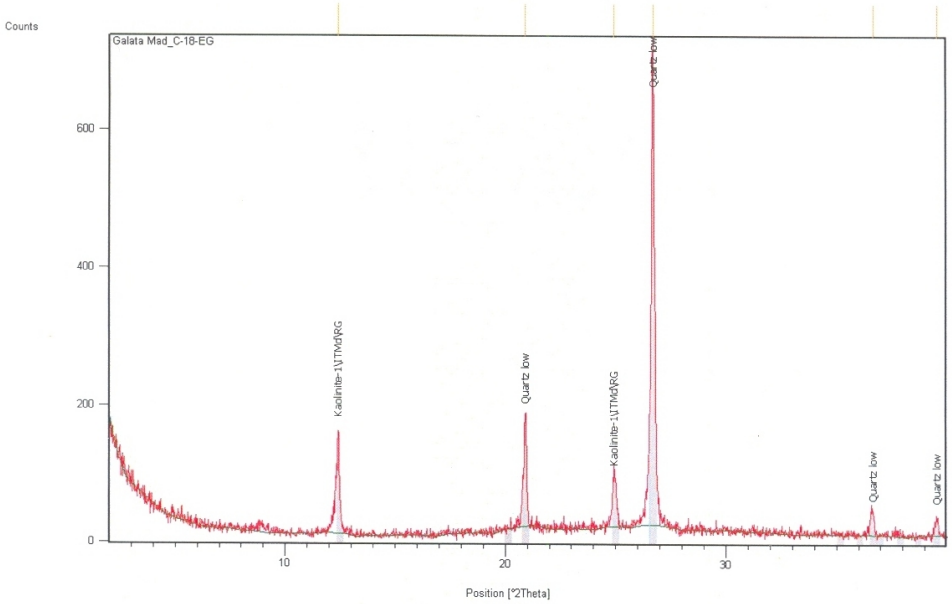
Counts
Galata Mad_C-18-EG
600
400
200
0
Kaolinite-1\1TM\RG
Quartz low
Kaolinite-1\1TM\RG
Quartz low
Quartz low
Quartz low
10
20
30
Position [°2Theta]

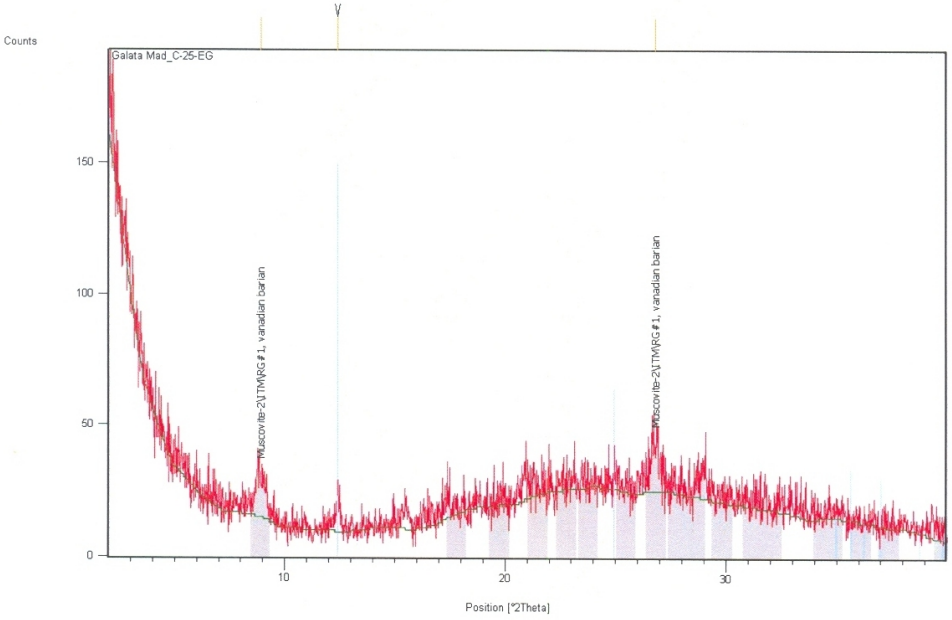
Counts
Galata Mad_C-25-EG
150
100
50
0
Muscovite-2\1TM\RG#1, vanadian barian
Muscovite-2\1TM\RG#1, vanadian barian
10
20
30
Position [°2Theta]

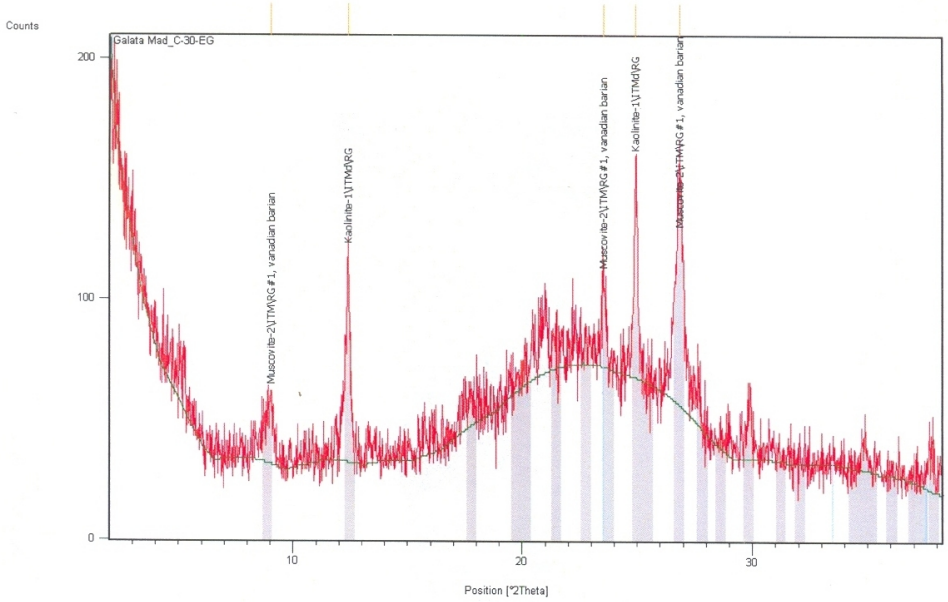
Counts
Galata Mad_C-30-EG
200
100
0
Muscovite-2\TMRG #1, vanadian barian
Kaolinite-1\TMRG
Muscovite-2\TMRG #1, vanadian barian
Kaolinite-1\TMRG
Muscovite-2\TMRG #1, vanadian barian
10
20
30
Position [°2Theta]

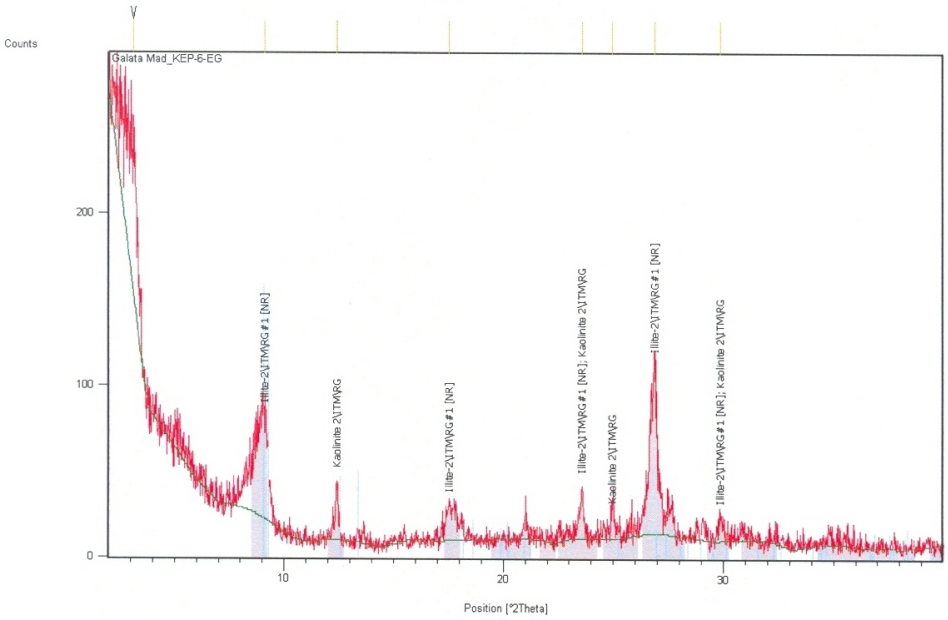
Counts
Galata Mad_KEP-6-EG
200
100
0
Illite-2\TMRG #1 [NR]
Kaolinite 2\TMRG
Illite-2\TMRG #1 [NR]
Illite-2\TMRG #1 [NR]; Kaolinite 2\TMRG
Kaolinite 2\TMRG
Illite-2\TMRG #1 [NR]
Illite-2\TMRG #1 [NR]; Kaolinite 2\TMRG
10
20
30
Position [°2Theta]

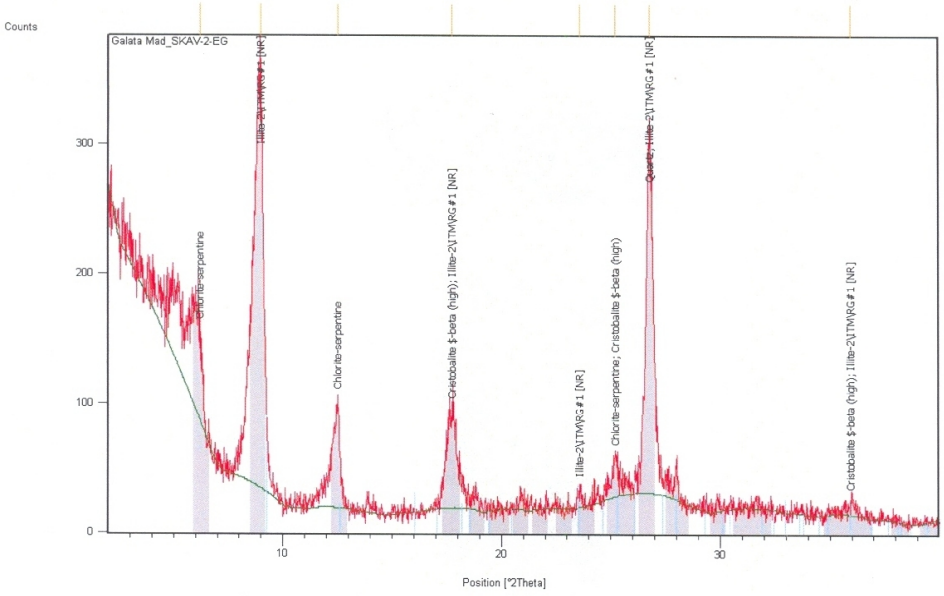
Counts
Galata Mad_SKAV-2-EG
Chlorite-serpentine
Illite-2\1TMXRG#1 [NR]
Chlorite-serpentine
Cristobalite $-beta (high); Illite-2\1TMXRG#1 [NR]
Illite-2\1TMXRG#1 [NR]
Chlorite-serpentine; Cristobalite $-beta (high)
Quartz; Illite-2\1TMXRG#1 [NR]
Cristobalite $-beta (high); Illite-2\1TMXRG#1 [NR]
300
200
100
0
10
20
30
Position [°2Theta]

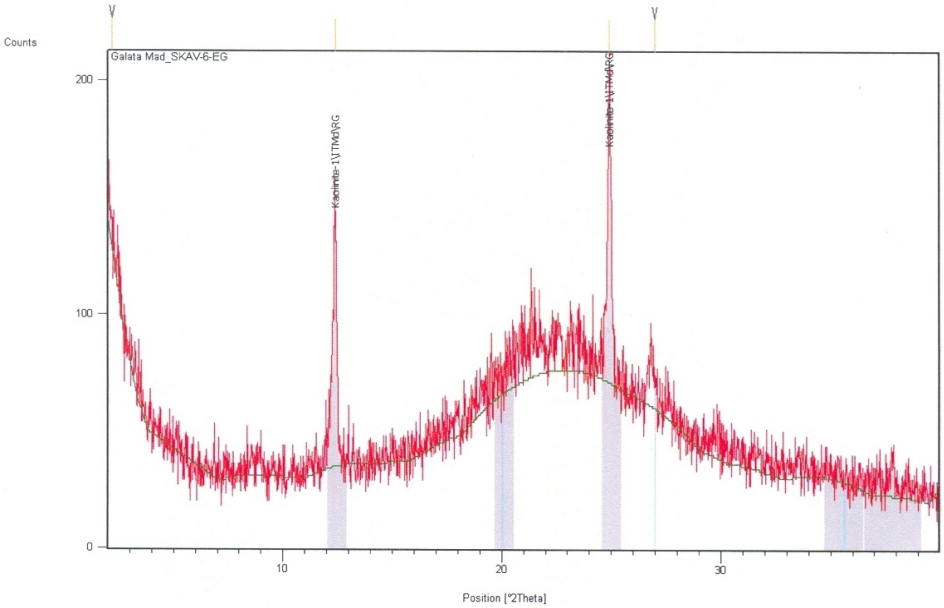
Counts
Galata Mad_SKAV-6-EG
Kaolinite-1\1TMXRG
Kaolinite-1\1TMXRG
200
100
0
10
20
30
Position [°2Theta]